ANALYSIS OF ABSORBER OPERATIONS FOR THE 5 KW AMMONIA/WATER COMBINED CYCLE

By

SIRISHA DEVI GOVINDARAJU

A THESIS PRESENTED TO THE GRADUATE SCHOOL
OF THE UNIVERSITY OF FLORIDA IN PARTIAL FULFILLMENT
OF THE REQUIREMENTS FOR THE DEGREE OF
MASTER OF SCIENCE

UNIVERSITY OF FLORIDA

2005

This work is dedicated to my parents.

ACKNOWLEDGMENTS

This thesis would not have seen the light without the help and support of many people. I would like to take this opportunity to thank all the people who made this possible.

I would like to express sincere gratitude to my advisor, Dr. Herbert (Skip) Ingley, who is a person with remarkable affability. He not only provided the necessary guidance and allowed me to develop my own ideas but also improved my people skills. I feel fortunate in getting the opportunity to work with him. I also appreciate my committee members Sherif A. Sherif and D.Yogi Goswami for the time and help they provided. I would also like to extend my gratitude to Dr. Dale W. Kirmse for his valuable discussions. I thank Dr.James Klausner and Dr.Lewis E Johns for their suggestions.

I greatly appreciate the discussions held with Nitin Goel, a doctoral student of Dr.Goswami. I would like to thank all my friends for their support and encouragement. My special thanks go to my special friend, Balachandran, for his ideas. Finally I would like to thank my parents for their love and inspiration, my brother, Dr. Sridhar Govindaraju and sister-in-law, Sirisha, for motivating me and keeping my spirits up all the time.

TABLE OF CONTENTS

APPENDIX

LIST OF TABLES

LIST OF FIGURES

NOMENCLATURE

a	Specifc area of packing (1/m)
A_i	Interfacial area (m^3/ m^2)
A_p	Projected Area (m^2)
A_s	Surface Area (m^2)
A_t	Area of tower (m^2)
C_p	Specific heat at constant pressure (KJ/kmoleK)
C_{sb}	Capacity parameter (m/s)
d	Diameter (m)
D	Diffusivity (m^2/s)
D_h	Hydraulic diameter
D_t	Diameter of tower (m^2)
G	Gibb's free energy (KJ/kg)
f_N	Natural frequency (1/s)
F_{lv}	Liquid flow parameter
F_{ro}	Froude's number
g	Acceleration due to gravity (m/s^2)
H	Enthalpy (J/kg)

H_2O	Water
K	Mass transfer coefficient (kmole/m^2)
m	Mass flow rate (kg/s)
M	Molecular weight(kg/kmole)
N	Molar flux (kmole/m^2s)
NH_3	Ammonia
P	Pressure (Pa)
Pr	Prandtl number
$Q_{v/o}$	Volume flow rate of gas per orifice (m^3/s)
Q_t	Volume flow rate of gas (m^3/s)
Re	Reynold's number
S	Specific entropy (KJ/kg K)
Sc	Schimdt's number
St	Stanton number
T	Temperature (^{o}K)
$u_{L,min}$	Minimum liquid load in packed columns (m/s)
V	Velocity (m/s)
V_{vf}	Flooding vapor velocity (f/s)
υ	Specific volume (m^3/kg)
x	Mass fraction of ammonia (kg/kg)

Greek

ρ	Density (kg/ m^3)

σ	Surface tension (N/m)
ε	Gas hold-up
η	Thermal conductivity (W/mK)
μ	Dynamic viscosity (Pa s)

Subscripts

awL	Ammonia/water liquid
L	Liquid
v	Vapor
B	Bubble
o	Orifice
sb	small bubble
trans	Transition from homogeneous to heterogeneous phase
lb	Large bubble
c	coolant
NH_3	Ammonia
H_2O	Water
i	Interface

Abstract of Dissertation Presented to the Graduate School
of the University of Florida in Partial Fulfillment of the
Requirements for the Degree of Master of Science

ANALYSIS OF ABSORBER OPERATIONS FOR THE 5 KW AMMONIA/WATER COMBINED CYCLE

By

Sirisha Devi Govindaraju

August 2005

Chair: H. A. (Skip) Ingley
Major Department: Mechanical and Aerospace Engineering

This thesis presents the analysis of absorber operations for the University of Florida's 5 KW ammonia/water combined cycle. As the absorber is a critical component of the combined cycle, its design and configuration play an important role in the performance of the cycle. The falling film absorber, tray/plate column absorber, bubble absorber, spray absorber and packed column absorber are the five configurations that are discussed in relation to the combined cycle.

The prescribed design conditions involve the ratio of the flow rate of weak solution to the vapor to be as high as 20:1. The required amount of ammonia to be absorbed into the weak solution can be as low as 3%. Based on these conditions, the various configurations of absorber were analyzed and it led to the conclusion that if the vapor is bubbled into the weak solution, then a large volume of the vapor will come in contact with the weak solution leading to better absorption.

An analytical model of the bubble absorber has been adapted to computer simulation that calculates the thermodynamic and transport properties of the ammonia/water mixture along with the design calculations. Although this model provides considerable insight into the theoretical operation of a bubble absorber, the assumptions required to run the model are questionable. Experimental analysis of the bubble absorber will be necessary to develop a more accurate model.

CHAPTER 1
INTRODUCTION

This chapter outlines the newly developed ammonia-water thermodynamic cycle, which is capable of producing both power and refrigeration.

Among the various refrigeration systems, the vapor compression and the vapor absorption systems are the most universally used systems. The compressor, condenser, expansion valve and the evaporator constitute the four main components of a vapor compression system. In a vapor absorption refrigeration system, an absorber-generator-pump assembly replaces the compressor of the vapor compression system. The input to the vapor compression system is in the form of high-grade energy (work) while in vapor absorption systems it is in the form of low-grade energy (heat). Examples of this source of heat include steam sources, hot exhaust gas and solar energy. This thesis focuses on the absorption system.

Two common variations of the absorption system are the lithium bromide/water ($LiBr/H_2O$) refrigeration system and the ammonia/water (NH_3/H_2O) refrigeration system. The latter system in which water (H_2O) is the absorbent and ammonia (NH_3) is the refrigerant is capable of achieving lower refrigeration temperatures than the former system in which water is the refrigerant. The ammonia/water refrigeration system is a major component in the combined cycle.

A new combined power and refrigeration thermodynamic cycle was proposed by D. Yogi Goswami in 1995 (as cited in Tamm[59]). This cycle combines the Rankine and absorption refrigeration cycles, using an ammonia/water binary mixture.[57] For a given

pressure, binary mixtures boil at variable temperatures while pure substances boil isothermally. The changes in the concentration of the working fluid, which is the liquid, account for the variable boiling temperatures of a binary mixture.[39]In such a process, during heat addition, the temperature difference between the heat source and the working fluid remains small when compared to the constant temperature boiling process. Thus more heat is extracted from the heat source resulting in less exergy loss and improved cycle performance.[59, 22] Hence the binary mixture with variable boiling temperatures yields a better thermal match with sensible heat sources than a pure substance which boils at constant temperature.[59]

The binary mixture of ammonia/water is used in the combined cycle because of its "desirable thermodynamic properties"[59] such as large heat capacity. Moreover ammonia is cheap when compared to other refrigerants and it is immiscible with lubricating oil. Though ammonia can be harmful to humans in concentration exceeding 50ppm, it is environmentally friendly and does not affect the ozone layer or contribute to global warming.

Figure 1.1 illustrates a schematic of ammonia/water combined cycle. The low-pressure saturated ammonia/water mixture in the absorber is pumped to a higher pressure and then is split into two streams, one of which passes through the rectifier (secondary stream) and the other (primary stream) passes through the recovery heat exchanger. In the recovery heat exchanger, the primary stream recovers the heat from the water-rich ammonia/water mixture coming back from the boiler. The secondary stream that passes through the rectifier takes away the heat from the ammonia vapor that is entering the rectifier through the boiler and helps in the condensation of any water remaining in the

vapor. In the boiler, the ammonia/water solution, which is rich in ammonia, is boiled to separate it from the weak ammonia/water solution and the ammonia-rich mixture passes through the rectifier before it passes through the superheater. Rectification helps in purifying the ammonia mixture, i.e, any water vapor present is condensed and returned to the generator. By superheating the ammonia vapor leaving the rectifier, the corrosion effects on the turbine blade are reduced and the refrigeration effect is increased. This superheated ammonia vapor is passed through the turbine where work is extracted. As the ammonia vapor expands in the turbine, it drops in temperature. The cold vapor is used in the refrigeration heat exchanger (cooler) to provide cooling. This cold, low-pressure ammonia vapor then flows into the absorber where in it is absorbed by the water-rich ammonia solution before being pumped back to the boiler. The water-rich ammonia solution leaves the boiler at a very high temperature. A part of its heat is recovered in the recovery heat exchanger and it is further passed through a pressure-reducing valve to reduce its pressure to absorber pressure. The pressure reducing valve ensures that the pressure difference between the absorber and the generator is maintained and the solution flows from the generator into the absorber and not vice-versa.

The recovery heat exchanger cools the weak solution while heating the strong solution before entering the boiler. This results in a decrease of heat input to the generator and heat rejection from the absorber and thus increases the overall cycle efficiency.

Goswami and Xu (1999) stated that the cycle can use source temperatures lower than 100°C, thus making it a useful power cycle for low cost solar thermal collectors, geothermal resources and waste heat from existing power plants.[21]

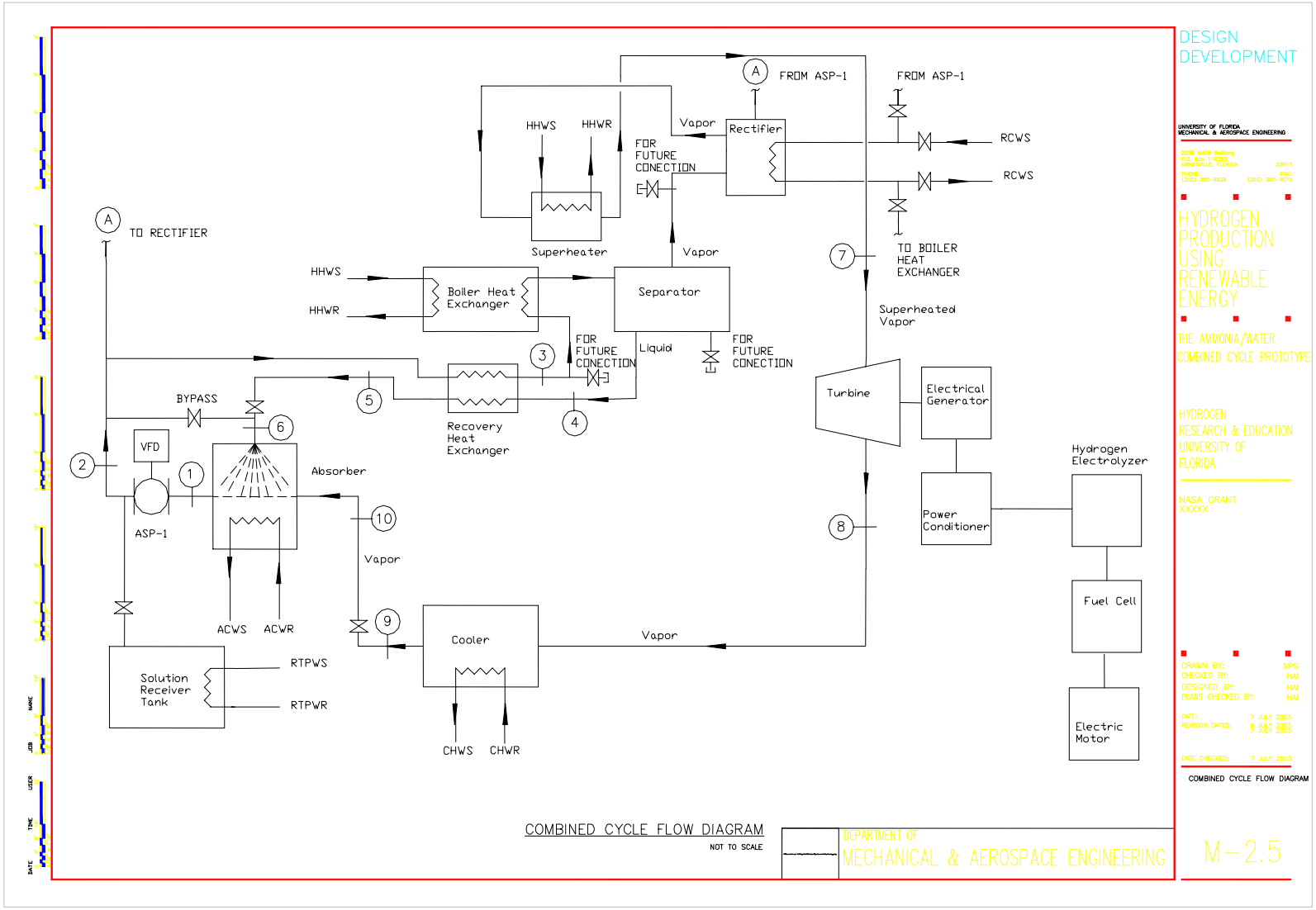

Figure 1.1. Combined ammonia/water cycle

The absorber being one of the principal components of the system plays a significant role in the working of this new cycle. The function of an absorber is to enhance the concentration of the weak refrigerant solution (NH_3+H_2O) by absorbing the vapor of the refrigerant (NH_3). In order to enhance the performance of the absorber, researchers have extensively studied the variant designs of absorbers. A summary of these studies is given in Chapter 2 and 3.

CHAPTER 2
BACKGROUND

Absorption, distillation, rectification, stripping, evaporation, humidification and dehumidification are a few techniques that involve contact between heterogeneous phases like liquid and gas.[46] Hence the systems used to carry out these operations are known as liquid-gas contacting systems and they involve transfer of mass, heat and momentum between the phases.[46] An absorber is one such liquid-gas contacting system, which is utilized for transferring both mass and heat between the phases involved. Therefore it can be referred to as a combined heat and mass exchanger which absorbs the vapor phase in a liquid absorbent and transports the vapor phase to the high-pressure side of the absorption cycle.[19]

The absorber is an important device in an ammonia/water absorption refrigeration system where ammonia is the refrigerant and water is the absorbent. In the absorber, the ammonia/water solution absorbs the ammonia vapor thus generating heat of absorption, which is transferred to a cooling fluid. At the University of Florida, this ammonia/water refrigeration system has been integrated with a Rankine cycle to produce a combined cycle that is capable of producing power and refrigeration.

As the absorber is a critical component of a vapor absorption system; the size, performance and cost of the absorber significantly influences the efficiency of the overall cycle. The performance of an absorber depends on the rate of absorption and the removal of the heat generated.[45] The rate of absorption is determined by the diffusion of ammonia vapor through the liquid phase and the flow of coolant affects the rate of removal of the

heat generated due to absorption.[45] If the flow of coolant is low, then the heat of absorption accumulates resulting in decreased mass transfer due to the increased vapor pressure.[45] Increasing the contact area between the ammonia vapor and the absorbent though the liquid phase enhances the diffusion of ammonia vapor. Hence, while designing an absorber, emphasis is placed on enhancing the heat exchange mechanisms and techniques to increase the absorption rates.

Principle of operation for liquid-gas contacting systems: The process equipment (described in greater detail in Chapter 3) utilized in a liquid-gas contacting system is designed based on the combination of working principles of three classes:[46]

1. Mode of flow of liquid and gas streams which can be one of the following:
    - Counter current flow
    - Co-current flow
    - Cross flow
2. Gross mechanism of heat and mass transfer which can either be differential or integral. In the differential mode, the system is divided into several elements. The control volume analysis of a single element is carried out by solving the governing equations where as in an integral mode the system is analyzed based on the overall conditions existing at the inlet and the exit.
3. The continuous phase can be that of gas or liquid.

Counter current flow: In counter current flow, liquid and the gas flow in opposite directions. In tray/plate columns operating on counter current flow, the tray occupies the entire cross section of the column as shown in Figure 2.1.[46] In such a case there are no downcomers* and the liquid and the gas flow through the same openings on the tray.[46]

* Downcomer: In tray columns, the liquid moves from one tray to the other either through the perforations on the tray or by downcomers/down spouts. They may be circular pipes or portions of tower cross section set aside for liquid flow by vertical plates[61]

Table 2.1. Characteristics of liquid-gas systems

Process Equipment	Mode of flow	Mechanism of heat and mass transfer	Continuous phase	Primary process applications
Tray/Plate column	Cross/Counter current	Integral	Liquid	Absorption Rectification Stripping
Packed column	Counter current/ Co-current	Differential	Liquid/gas	Absorption Rectification Stripping Humidification Dehumidification
Falling film/Wetted wall column	Counter current/ Co-current	Differential	Liquid/gas	Absorption Rectification Stripping Evaporation
Spray chamber	Counter current/ Co-current/Cross	Differential	Gas	Absorption Stripping Humidification Dehumidification

*Adopted from Perry and Chilton, Chemical Engineer's Handbook, Fifth Edition, McGraw Hill, New York 1973.[46]

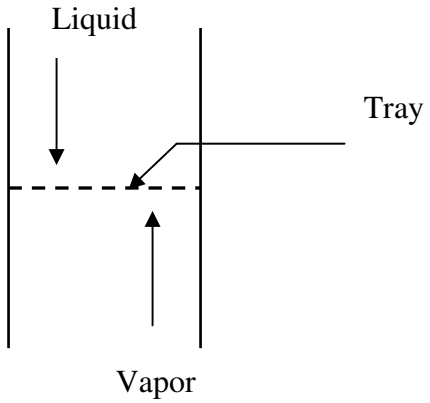

Figure 2.1. Counter current flow

Based on the application of counter current flow in tray columns, the counter current trays are further classified as

1. Dual-flow tray

Dual- flow trays are trays with usually simple round perforations in the range of 1/8 inch to ½ inch.[46] The entire area of the tray is perforated with holes. As the vapor and

liquid flow counter-currently through the perforations, it is known as dual flow.[28] Liquid flows downward momentarily through perforations whereas vapor flows upward through perforations. These devices have a very narrow range of operating efficiency.[28]

2. Turbo-grid tray

This is a tray with long slot openings. The width of these openings is in the range of ¼ to ½ inch.[46] These trays are useful in handling liquids with suspended particles.[61]

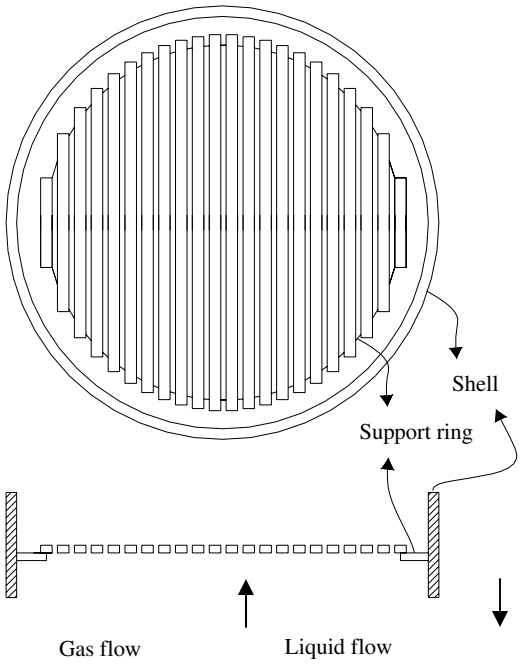

Figure 2.2. Turbo-grid tray

3. Ripple tray

The tray material is wavy to partially segregate the gas and liquid flow and hence it is known as a ripple tray.[46] The continuous agitation of the liquid on the top side of the trays along with the continuous underside wetting or washing action makes this tray ideal for potentially fouling services.

4. Baffle tray/shower deck

The arrangement of the tray is either flat or it slopes slightly in the direction of liquid flow.[46, 28] In this case, the liquid flow is dispersed but the flow of the gas is continuous.[46] The gas comes in contact with the liquid as the liquid flows down the tray. This is used widely when the liquid contains solids.[46, 28]

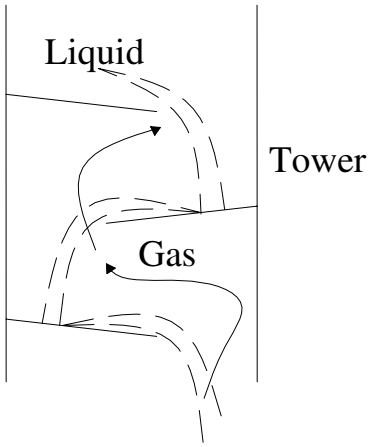

Figure 2.3. Flow in a tower utilizing baffle plate

Cross flow: In cross flow, the liquid flow is across the gas flow. In tray/plate columns operating on cross flow, the tray occupies only a certain percentage of the tower area as shown in Figure 2.4 and the rest of the area is utilized as the downcomer area which helps the liquid to flow from one tray to the other. The liquid downcomer helps in controlling the liquid flow pattern and this leads to stability of liquid flow and higher mass transfer efficiency. The cross flow is used more often than the counter current flow because of greater operating range and better transfer efficiencies.[46]

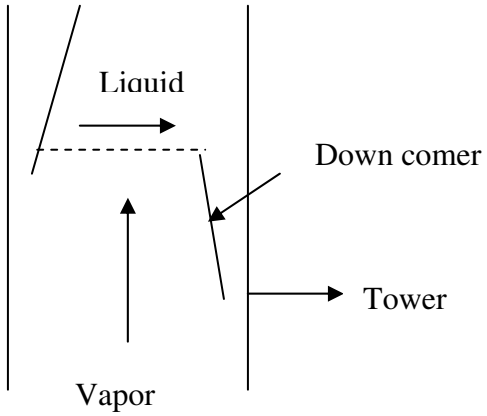

Figure 2.4. Cross flow

The common categories of cross flow plates based on the mode of liquid flow are: [46, 52]

1. Cross flow tray

The liquid flows directly across the tray (cross flow). It is the most economical to fabricate. Its high efficiency is due to the long liquid path.

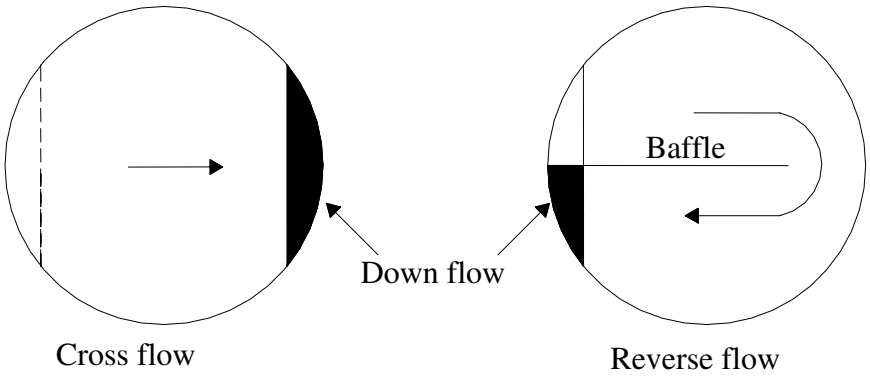

Figure 2.5. Cross sectional views of towers operating with cross flow and reverse flow

2. Reverse flow tray

All the downcomers are located on one-side of the column and the liquid is forced to flow around a center baffle, reversing its direction at the other end of the tray. This minimizes the downcomer area and increases the area that can be used for gas dispersion. The long liquid path might result in high liquid gradients. It is more suited for low liquid/vapor ratios.

3. Double pass tray

The liquid flow is split into two portions and each flows across half of the tray. The arrows in Figure 2.6 show the direction of the liquid flow. It can handle higher liquid flow rates and hence it is suited for large liquid/vapor ratios. But the shorter liquid path results in a lower efficiency for the double pass when compared to the cross flow mode.

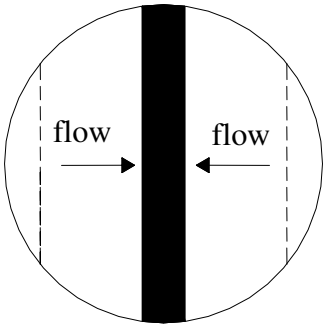

Figure 2.6. Cross section of a double pass tray

4. Double pass, cascade tray

For higher liquid flows, the tray floor is stepped at two elevations along with splitting the liquid flow into two portions. This is known as double pass, cascade tray.

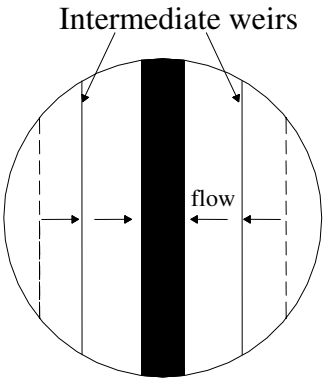

Figure 2.7. Double pass cascade tray

5. Four pass tray

This is similar in construction to double pass. The liquid is split into two portions each of which is again split into two more portions as shown in Figure 2.8. This is suited for larger diameter towers. As the liquid flow length is cut short, the efficiency decreases.

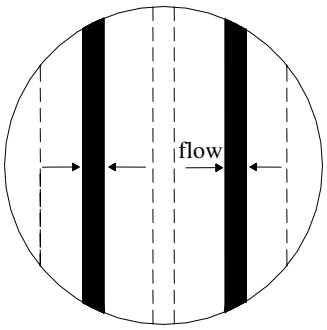

Figure 2.8. Four pass tray

Table 2.2. Criteria for selecting cross flow pattern

Estimated tower diameter (feet)	Range of liquid capacity (gal/min)			
	Reverse flow	Cross flow	Double pass	Cascade double pass
3	0-30	30-200	Not applicable	Not applicable
4	0-40	40-300	Not applicable	Not applicable
6	0-50	50-400	400-700	Not applicable
8	0-50	50-500	500-800	Not applicable
10	0-50	50-500	500-900	900-1400
12	0-50	50-500	500-1000	1000-1600
15	0-50	50-500	500-1100	1100-1800
20	0-50	50-500	500-1100	1100-2000

*Adopted from Design of Equilibrium Stage Process, Chapter 14, Smith, Mc Graw Hill, New York, 1963.[52]

Co-current flow: In co-current flow, the flow of liquid and gas is in the same direction.[46] Both liquid and gas flow downwards. As the flow is in the same direction, the pressure drop in the towers with co-current flow is much less when compared to the towers with cross and counter current flow. The liquid and the gas flow in the same direction and as a result the contact time and interfacial area between the two phases is decreased in this case. Hence the rate of absorption declines, resulting in lower transfer efficiencies. They are efficient only when there are large absorption driving forces available.

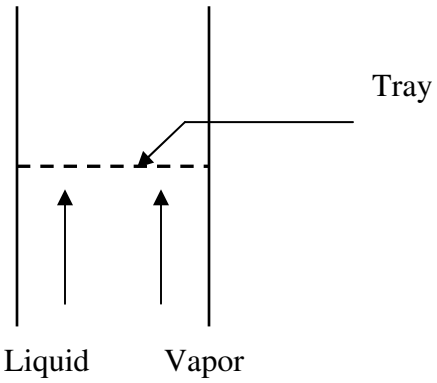

Figure 2.9. Co-current flow

The intention of the current study is to analyze the absorber and its performance in reference to the combined cycle and hence absorption was the primary process application that was considered. Based on the principles described in section 2.1, different absorber configurations have been designed by researchers. These configurations are described in Chapter 3.

CHAPTER 3
LITERATURE REVIEW

In support of the research currently in progress at the University of Florida regarding the ammonia/water combined cycle, this thesis focuses on the performance of the absorber, an integral part of the combined cycle. Different designs of absorber have been explored and a summary of these designs is described below.

3.1 Packed Column Absorber

Packed column absorbers consist of a tower filled with packings made of metal, ceramic, glass or plastic along with a support plate for the packing material and a liquid distributing device.[46] The packings can be randomly dumped in the column or they can be structurally arranged. The liquid from the liquid distributor flows down through the packings and the gas flows up resulting in contact between the liquid and the gas phases. These columns are extensively used for absorption although they can also be used for rectification, humidification and dehumidification operations3. A single column can have several packed beds.

The packings in a packed column enhance the contact /interfacial area between the liquid and the vapor. This results in increased diffusion of the vapor into the liquid and subsequently higher absorption rates. But the packed column has no arrangement to incorporate coolings coils and hence removal of heat of absorption is difficult.[46]

A. M. Selim and M. M. Elsayed[49] investigated the performance of a packed bed absorber at various operating conditions. Their study showed that changing the operating pressure of the bed did not affect the performance of the bed while increasing the bed

height resulted in enhanced absorber efficiency. It was noted that beyond a certain height of the bed, the changes in the efficiency were negligible. This height is defined as the effective bed height. They found that an increase in height further than the effective height would only result in higher pressure drop across the bed and higher operating costs. They also reported that when ceramic berl saddles are used instead of ceramic rasching rings, the rate of mass absorption increased from 5% to 8% of the value given by ceramic rasching rings but this depends on the flow rate of the solution and the vapor.

A. M. Selim and M. M. Elsayed[49] also proposed and investigated the performance of a two-stage packed bed absorber for an ammonia/water absorption system. Their results show that multi-stage absorption while cooling the weak solution in between the stages increases the rate of absorption. But this arrangement would further increase the cost, size and complexity of the absorber.

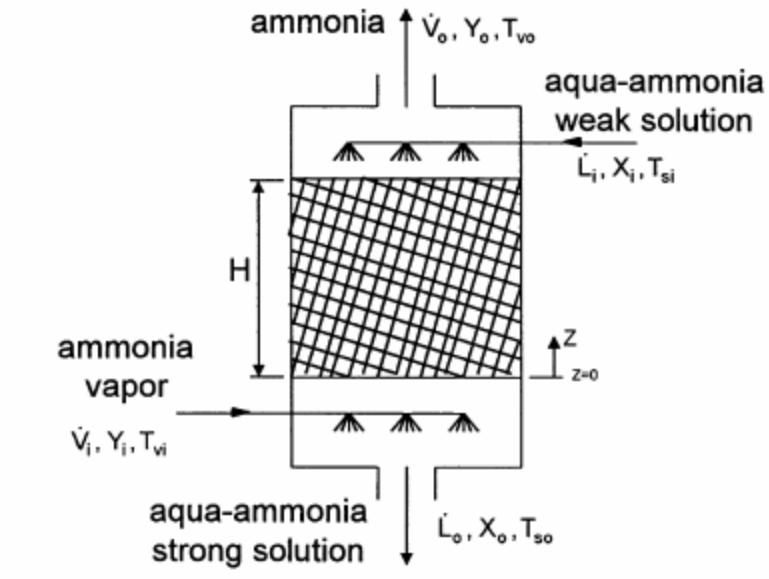

Figure 3.1. Packed bed absorber

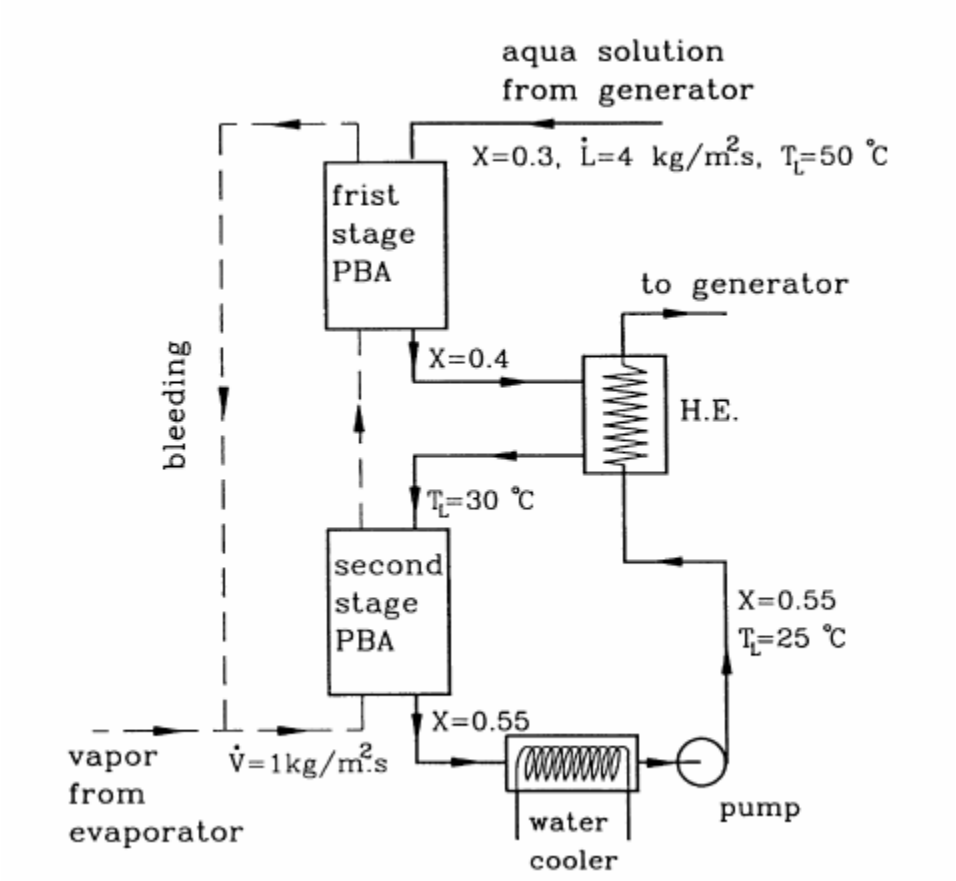

Figure 3.2. Two-stage packed bed absorber

Packings can be made of ceramic or other resistant material. Hence acids and corrosive materials can be handled in packed columns.[46] Robert H. Perry and Cecil H. Chilton state that the liquid agitation is low in packed columns and hence liquids tending to foam can be more readily handled in these columns. But low liquid rates result in incomplete wetting of the packings, consequently the contact area between the vapor and the liquid decreases.[46] Hence packed columns are not preferred when the liquid flow rates are low. The minimum liquid load for packings can be estimated using equation 3.1.[54]

$$u_{L,\min} = 7.7 \times 10^{-6} \times \left(\frac{\rho_L \sigma^3}{\mu_L^4 g} \right)^{2/9} \left(\frac{g}{a} \right)^{1/2} \qquad (3.1)$$

If the packing consists of extended surfaces, then there is a decrease in the orifice area through which the liquid can flow. As a result there will be a buildup of a continuous liquid column. This results in flooding which reduces the efficiency of the absorber. In Mass transfer operations written by Robert E. Treybal[61], it is mentioned that if packed columns are used for larger diameters (> 2 feet) then redistribution of liquid is a problem. However if structured packings are used, then packed columns can be used for very large diameters.

3.2 Falling Film/Wetted Wall Column Absorber

The concept of packed columns can be slightly modified by replacing the packing with heat transfer surfaces like vertical or horizontal tubes. This arrangement is known as a falling film absorber. The liquid absorbent flows down as a film on the tubes due to gravity while the vapor flows in a direction opposite to the liquid flow and is absorbed into the liquid film flowing over the tubes. The heat of absorption is rejected to the coolant flowing through the tubes. However the falling films have wettability problems and they require liquid distributors to distribute the liquid.[35] The mass transfer process in the falling film controls the absorption rate.[45] The flooding of adjacent surfaces is a major concern in falling film absorbers.[19] In spite of these difficulties, the falling film is widely used due to the low-pressure drops in the vapor and the liquid phase.[19]

In order to enhance the performance of the falling film configurations, the conventional design with cylindrical tubes has been revised, different surface structures have been added to the tubes over which the absorbent flows down as a film and the properties of the absorbent have been modified.

Variations in falling film absorbers: The properties of the absorbent can be modified by the addition of surface-active chemical agents. These chemical agents help

in the generation of turbulence at the surface of the falling film, which in turn improves the rate of diffusion between the vapor and the absorbent. This increased rate of diffusion results in higher absorption rates.[27] Moreover the addition of surfactants to the solution results in a decrease of the surface tension and as a result the wettability is increased.[43] Moller and Knoche[41] investigated the influence of surfactants like anionic, non-ionic tensides and l-octanol on an ammonia-water refrigeration system. It was found that 1-octonol had a significant influence on the absorption rates while anionic and the non-ionic tensides had no effect on the mass transfer process. But it is difficult to find surfactants that are chemically stable at higher temperatures. The wettability can also be improved by surface treatment, which can be shape treatment or roughness treatment.[43] The shape treatment is categorized as macroscale treatment where as the roughness treatment is classified as the microscale treatment. The constant curvature surface(CCS) is one of the macro scale treatments. The CCS has been studied by Isshiki et al. (as cited in Goel[19]) and they reported the formation of a uniformly thick falling film around these surfaces. The results also showed that the heat transfer is improved in this case as compared to the rectangular and the triangular fins. However, CCS tubing is not cost-effective due to its high manufacturing cost.[43] In order to increase the wettability on the surface, microscale treatments such as scratching, coating and baking (oxidation) were investigated. Park et. al.[43] tested a bare tube and two-different microscale hatched tubes and found that the absorption performance in the microscale hatched tubes with roughness in the range of 0.386-6.968 μm increased twofold over than that of a bare tube. The improvement in the absorption performance is due to the increased wettability which promotes higher heat transfer between the solution and the coolant.

Kang and Christensen used rotating cylinders in order to increase the heat transfer mechanism in a falling-film absorber of a Li-Br absorption system. Figure 3.3 shows the arrangement of the rotating cylinder – absorber using two concentric cylinders. The outer cylinder is held stationary while the inner cylinder rotates about its axis. The weak solution of Li-Br is injected into this rotating inner cylinder while the coolant flows axially in the annular region. As the cylinder rotates, the centrifugal force causes the weak solution to form a thin film on the periphery of the inner cylinder resulting in increased area of contact between the weak solution and the coolant. Apart from the

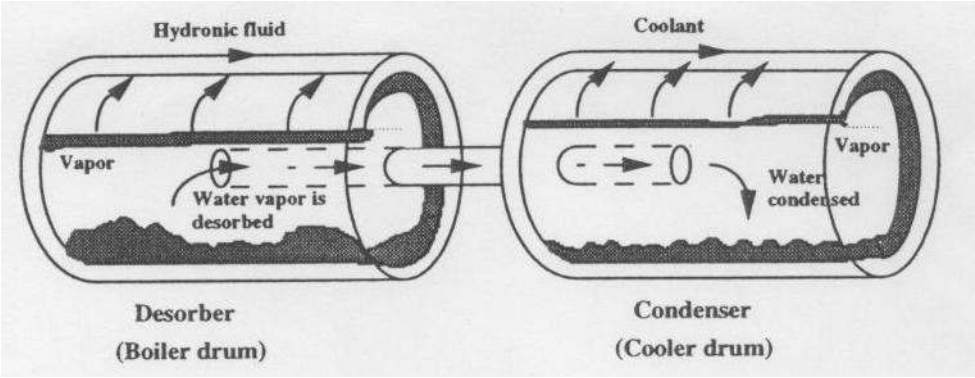

Figure 3.3. Arrangement of rotating cylinders in falling film

increased contact area, the rotation promotes turbulence. As a consequence of this, the heat transfer mechanism is enhanced and the absorption rate increases. However this arrangement requires additional energy to run the cylinders and hence its application is restricted to small absorption systems.

Earlier studies show that there will be significant improvement in the heat transfer mechanism when an axially fluted tube is used instead of a simple cylindrical tube.[8] The surface area for a fluted tube is significantly higher when compared with a smooth cylindrical tube. A.T.Conlisk found that the heat transfer is enhanced only if the ratio of the total mass absorbed for the fluted tube to that of the smooth tube is greater than the

area ratio. Later on Conlisk analyzed the performance of a spine-tube absorber.[11, 12] But the geometry of a spine-tube is complicated and there is no significant improvement in

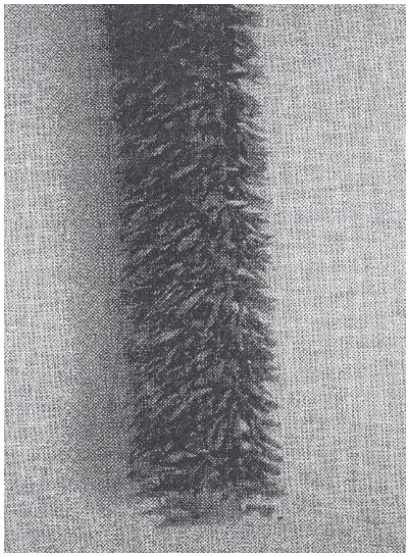

Figure 3.4. Spine tubes

the heat transfer. It was found that as the pitch between the spines is increased, the surface tension effects became significant and the heat transfer is decreased noticeably.

The surface structures like fins and protrusions that have been added will help in the formation of a stable liquid film over a larger section of the falling film. Siyoung Jeong et. al.[29] depicted the heat transfer performance of a coiled tube absorber. A coiled tube absorber consists of a coiled tube and a shell. The coiled tube is wound compactly minimizing the pitch as shown in Figure 3.5. The weak solution of ammonia/water flows downward over the outer and inner sides of the tube and the ammonia vapor is absorbed in it while the vapor is flowing upwards.

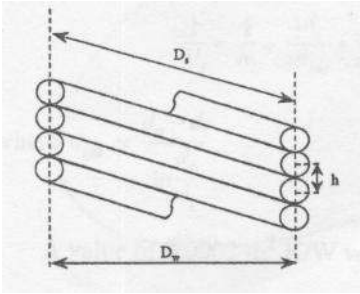

Figure 3.5. Arrangement of coils in the coiled tube absorber

The coolant that is flowing inside the coiled tube removes the absorption heat that is generated. The centrifugal force caused by the coolant flow through the tube gives rise to a secondary current in the form of a double vortex and as a result the turbulence is increased. This resulted in enhanced heat transfer between the coolant and the wall of the tube. Their experiments showed that the reduction of the radius of curvature and an increase in the number of turns in the coil lead to enhanced heat transfer. In this study, two sets of experiments were carried out, one experiment was with absorption (NH_3 and H_2O) and the other experiment was without absorption (only H_2O was used as the solution). The final conclusion of the study was that problems like stagnation of the liquid film caused by the shear force between the liquid and the vapor phase, locally thick films and insufficient wetting result in low heat transfer coefficients in experiments with absorption when compared with experiments without absorption.

3.3 Adiabatic Spray Absorber

The basic principle of an adiabatic spray absorber is to perform heat and mass transfer separated from each other in two different components. The heat is rejected in a heat exchanger while the mass transfer occurs in a simple vessel. This results in effective heat rejection along with high mass transfer.[56] Summerer et al. described the working of an adiabatic spray absorber with the working fluid as Li-Br. In this case, the Li-Br

solution is sub-cooled in the heat exchanger. A nozzle sprays this sub-cooled solution into an adiabatic chamber where water vapor is present. On absorbing the vapor, the solution is warmed up slightly and is diluted until equilibrium is reached both in temperature and concentration. A part of this weak solution is pumped to the generator to be regenerated again while the remaining solution is re-circulated. The spray absorber can work with fluids like hydroxides, which have low heat transfer coefficients. Hydroxides have a poor heat absorption in falling film absorbers and this is partly due to their high viscosity. The arrangement of an adiabatic spray absorber is shown in Figure 3.6.

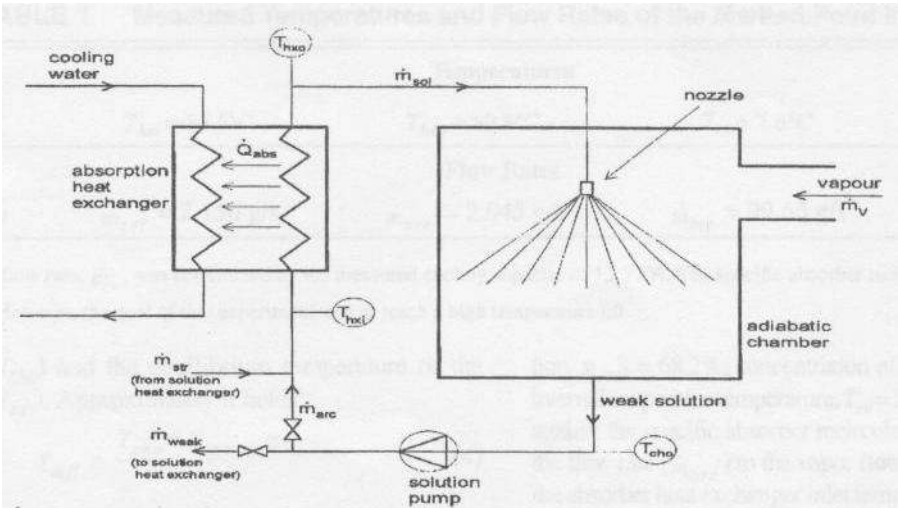

Figure 3.6. Spray absorber

In a spray absorber, a plate heat exchanger can be used. The plate heat exchanger is much cheaper when compared with the shell and tube heat exchanger. Hence the application of a spray absorber to low capacity systems will turn out to be cheaper and compact when compared to the falling film absorbers. However the results of the experiments conducted with the Li-Br solution showed that if the spray chamber has to be large (for machines with capacities >50 KW) then there is no significant difference in the

cost of spray absorber and falling film absorber. Moreover the nozzle should be carefully chosen in order to avoid high-pressure drops. Higher pressure drops result in higher pumping power.

3.4 Tray/Plate Column Absorber

A tray column absorber consists of several trays/plates that are enclosed in a cylindrical tower. In general, the mode of flow in tray column absorbers is cross flow. The gas flowing through the perforations is dispersed into the liquid that holds on the tray. This liquid hold-up results in a better contact between the liquid and the vapor. The downcomers help in the liquid to flow from the top tray to the bottom tray.

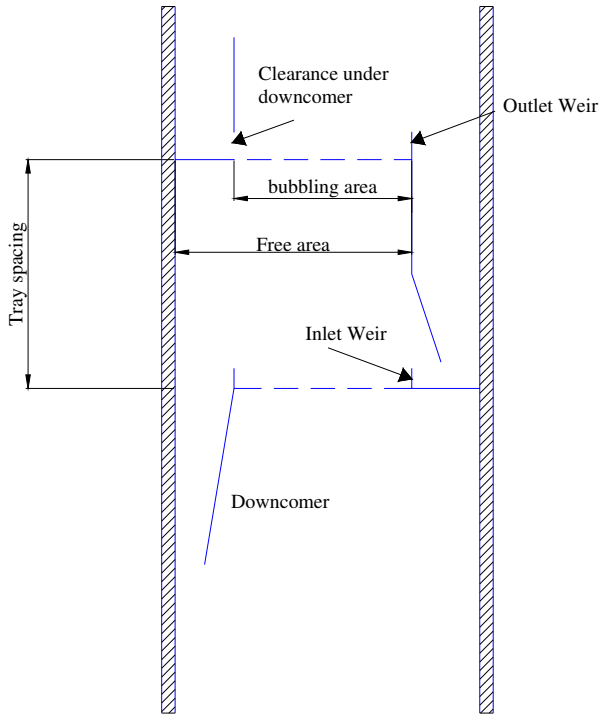

Figure 3.7. Tray terminology

In the Chemical Engineers Handbook[†46], by Perry and Chilton, it is stated that "the maximum allowable capacity of a plate for handling gas and liquid flow is of primary

[†] Page 18-5

importance because it fixes the minimum possible diameter of the column and the minimum allowable capacity of a column is determined by the need for effective dispersion and contacting of the phases."

In a tray column, increasing the gas flow while keeping the liquid flow rate constant results in entrainment of the liquid along with the gas in which case it would be difficult to maintain a net downward flow of liquid. This condition is known as entrainment flooding.[46] Similarly if the gas flow is kept constant and the liquid flow rate is increased then it results in a net downward flow of liquid. This condition is known as down flow flooding or weeping.[46] Weeping is indicated by increased pressure drop and reduced transfer efficiencies.[46]

Hence while designing a tray column, care should be taken about the down flow capacity of the liquid, allowed entrainment of liquid along with the gas and dispersion between the two phases. These parameters affect the transfer efficiency and as a result the absorber efficiency is affected. The tray column absorbers can be classified as:

1. Bubble cap absorber
2. Sieve plate absorber
3. Valve plate absorber

The bubble cap absorber is made up of trays with bubble caps. A bubble cap consists of a center riser and a cap.[46] The gas flows through the center riser and it reverses flow under the cap and passes downward through the annulus between the riser and the cap and then flows into the liquid on the tray through the openings/slots on the lower side of the cap. A built-in seal in the bubble caps prevents the liquid drainage at low gas flow rates. As a result of this bubble caps can operate at very low gas flow

rates.[46] There are many varieties of bubble caps but the round, bell-shaped bubble cap is the most commonly used cap.[46, 52] Bubble cap trays are one of the oldest technologies. However, they have been replaced by sieve trays/valve trays because of the ease of operation, low maintenance, high operating range and low cost factors of the sieve/valve plates. [52, 60]

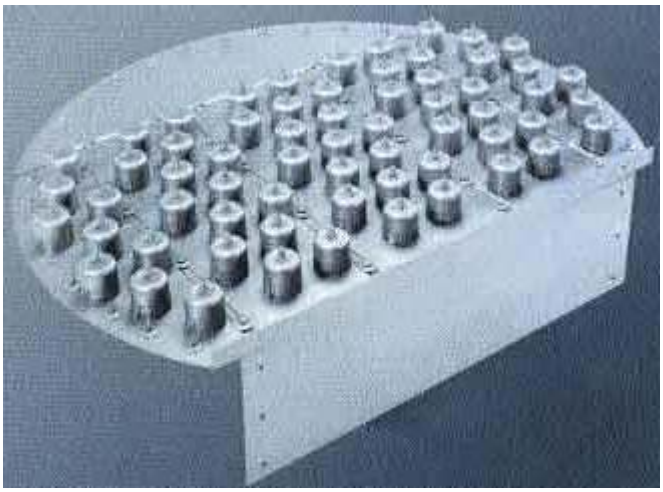

Figure 3.8. Single pass bubble cap tray

A sieve plate absorber employs a tower that consists of trays with simple orifices, which can be circular, square or rectangular. The flow of the gas prevents the liquid from flowing through the perforations.[46] But when the gas flow is low, it results in weeping and thereby mass transfer efficiency is reduced as the contact area between the gas and liquid is reduced. A large pressure drop in the column indicates weeping.

An absorber that encloses trays with movable valves that provide variable orifices of non-circular shape is known as a valve plate absorber. When the gas flow is low, the valve tends to close and hence the problem of weeping, which we see in sieve plate absorbers, is minimized in valve plate absorbers. The opening and closing of the valve helps in maintaining the dynamic pressure balance across the plate.[46]

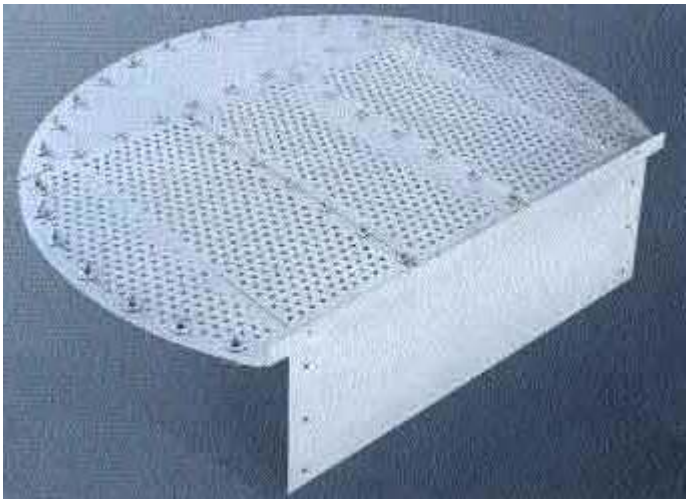

Figure 3.9. Single pass sieve tray

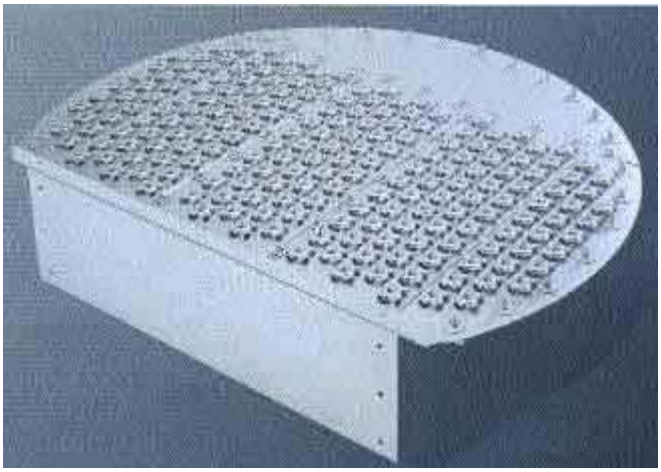

Figure 3.10. Single pass valve tray

Perry and Chilton stated that the tray column absorbers are preferred for tower diameters more than 2 feet but for tower diameters less then 2 feet, packed columns are preferred as they turn out to be cheaper than the tray column absorbers.[46]

3.5 Bubble Absorber

In a bubble absorber, the vapor bubbles through the weak solution either co-currently/counter currently. The vapor bubbles break as they are injected into the weak solution. This results in an increased interfacial area and as a result there is good mixing

between the vapor and the liquid phase. The bubble type heat transfer not only provides high heat transfer coefficient but also good wettability. It does require vapor distribution. In general vapor distribution is easier to accomplish than liquid distribution. However there is a large pressure drop in bubble absorbers. As a result the height of the absorber is restricted.

Many correlations are available in order to determine the initial bubble diameter. The correlation of Akita and Yoshida is mostly applicable for single orifice systems. However, Bhavaraju's correlation is the most widely used one. Recently, Kang et al.[35] visualized the bubble behavior for an ammonia/water bubble absorption system and their results show that the bubble dynamics such as bubble velocity and the bubble diameter play an important role in the enhancement of absorption performance. Also, their study determined that the orifice diameter, the orifice number, liquid concentration and vapor velocity are considered to be the key parameters in bubble absorption. Their results show that the initial bubble diameter (it is the diameter just before departure from the orifice) increases with the increasing orifice diameter and liquid concentration while the orifice number has no significant effect on the initial bubble diameter.[35] They came up with a new correlation for the initial bubble diameter.

Ferreira et al. developed a model of vertical tubular bubble absorber for an ammonia/water absorption refrigeration system. Their set-up consisted of three concentric tubes in which the inner most tube is generally the absorber while coolant flows in the other two tubes. It had been found that the major absorption process takes place in the slug flow region. With the help of the results from their experiments, they determined a correlation for the absorber height as a function of the initial conditions.

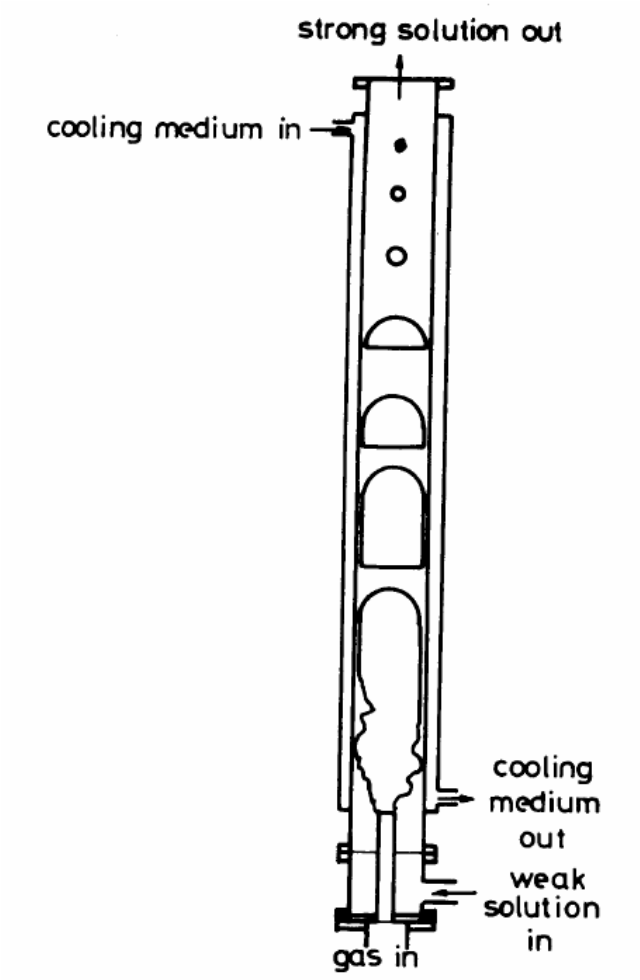

Figure 3.11. Vertical tubular bubble absorber

Herbine and Perez-Blanco studied a similar model of an ammonia/water tubular bubble absorber. Their model consists of two concentric tubes with solution and ammonia vapor flowing co-currently upward in the inner tube while the coolant flows downward in the outer tube. The ammonia vapor is injected into the inner tube with the help of an injector. Their results show that the direction of ammonia transfer is always from the bubble to the liquid. Water is transferred into the bubble first, but after equilibrium is reached at the interface, it has been found that the direction of water transfer reverses till the bubble disappears. They found that the interface temperature is lower than the liquid temperature when water transfers into the bubble while the interface

temperature is above the liquid temperature when the water transfers out of the bubble. Also they described the water mass transfer as a product of the ammonia mass transfer and the vapor phase's extent to equilibrium. However, the general practice is to find the water flux using the equilibrium relations at the liquid-vapor interface. The authors feel that further research needs to be done on this model in order to determine the effect of multiple injection points along the absorber length.

Kang et. al.[32] developed a model for bubble absorber with a plate heat exchanger by using combined heat and mass transfer analyses. They considered the heat and mass transfer resistances not only in the liquid region but also in the vapor region by solving diffusion and mass balance equations simultaneously. A schematic of the absorber is shown in Figure 3.12. The weak ammonia/water solution flows from the top on the inside of the plate heat exchanger while the vapor flows up through the orifices at the bottom of the heat exchanger in a direction opposite to the liquid flow. The hydronic fluid used as a coolant flows in the same direction as that of the vapor but on the outer wall of the inner side of the heat exchanger. They found that the liquid temperature is closer to the interface temperature of the vapor and the liquid while the vapor temperature is much lower than the interface temperature. Also, if the ratio of the ammonia molar flux to the total molar flux absorbed/desorbed is less than one, then both ammonia and water components were absorbed from the bubble into the liquid region. But when this ratio was greater than one the ammonia was absorbed into the liquid region while water was desorbed into the vapor region.

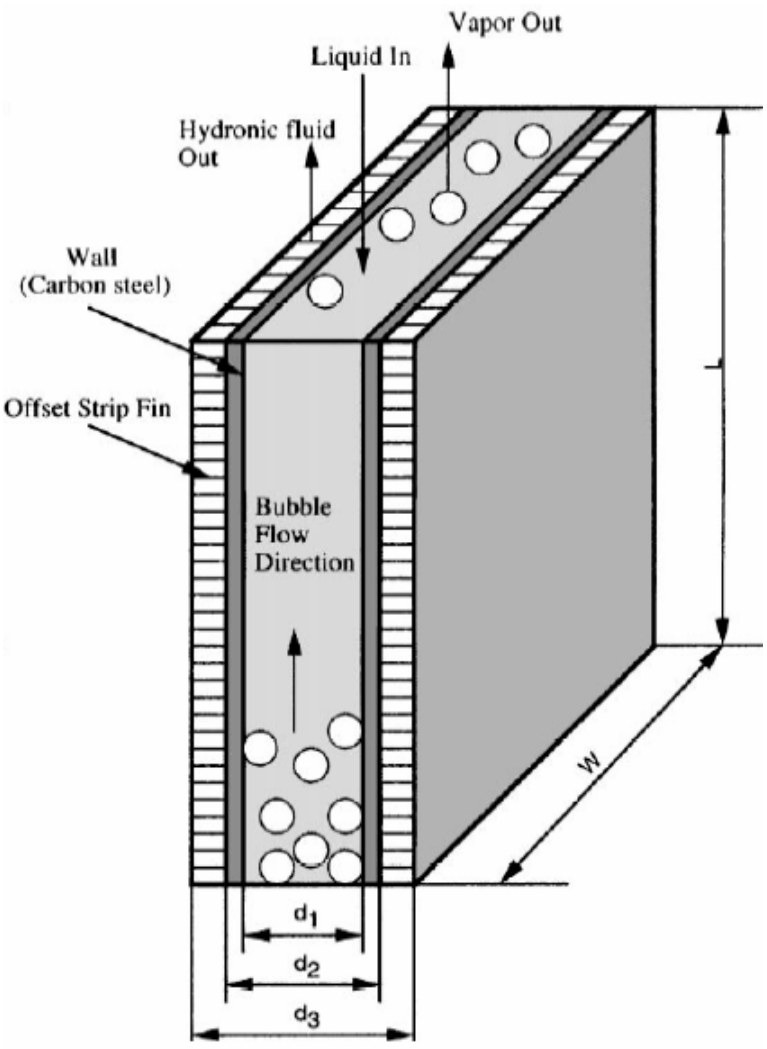

Figure 3.12. Bubble absorber

Their results show that the bulk liquid concentration was lower than the equilibrium concentration while the bulk vapor concentration was close to the equilibrium concentration which meant that the mass transfer resistance is dominant in the liquid region. But the heat transfer resistance was found to be dominant in the vapor region. They concluded that mass transfer area has a more significant effect on the size of the absorber. Increasing the distance between the two plates of the heat exchanger increases the mass transfer area and hence the size of the absorber decreases.

CHAPTER 4
MATHEMATICAL MODEL AND ANALYSIS

The construction of the packed column absorber, falling film/wetted wall column absorber, spray absorber, tray/plate column absorber and bubble absorber have been described in Chapter 3. Based on these configurations, the performance of a suitable absorber for the 5 KW ammonia/water combined cycle has been analyzed in this chapter.

The ammonia/water combined cycle creates electricity and cooling from a low temperature heat source. In order to generate 5 KW electricity in the generator constraints have been laid on the temperature and the pressure of the system. The high and the low pressure in the cycle have been fixed at 40 psia and 110 psia. The temperature exiting the boiler and the absorber are fixed at 170^{o}F and 100^{o}F. Based on these conditions, the other design conditions were calculated.

Table 4.1. Design conditions for the absorber[‡]

	SI		FPS	
Pressure	2.758×10^{5}	Pa	40	psia
Inlet conditions				
Weak solution mass flow rate	0.9389	kg/s	7452.31	lb/hr
Weak solution mass fraction	0.3696	kg/s	0.3696	lb/hr
Weak solution bulk temperature	318.56	°K	114	°F
Vapor mass flow rate	0.0469	kg/s	372.37	lb/hr
Vapor mass fraction	0.997	kg/kg	0.997	lb/lb
Vapor bulk temperature	302.44	°K	85	°F
Outlet conditions				
Solution mass flow rate	0.9859	kg/s	7824.68	lb/hr
Solution mass fraction	0.3996	kg/kg	0.3996	lb/lb
Solution bulk temperature	310.78	°K	100	°F

[‡] Calculations done by Robert Reed, Graduate Student, University of Florida, 2003-2005.

The design conditions show that the mass flow rate of the vapor (0.0469 kg/s) is very low compared with that of the weak solution (0.9389 kg/s). Moreover the desired increase in the ammonia mass fraction is only 3%. This shows that the major portion of the ammonia at the outlet of the absorber is from the weak solution.

The above observations play an important role in choosing the configuration of the absorber. As the vapor flow rate is very low in the 5 KW combined cycle system at the University of Florida, the entire vapor should come in contact with the weak solution in order to achieve an increase in the mass fraction of the ammonia. This led to the conclusion that if the vapor is bubbled through the weak solution, a large volume of the vapor comes in contact with the weak solution. Secondly, in order to keep this process continuous, the heat generated due to the absorption needs to be removed.

Among the various configurations discussed in the earlier chapter, the tray/plate column absorber, bubble absorber and the spray column absorber involve a bubble phase. The vapor bubbles out at multi-stages in a tray/plate column absorber. Hence this configuration was explored in a greater depth.

4.1 Design of a Tray/Plate Column Absorber

The design specification check list for the over-all tray/plate column design is shown in Table 4.2.[52] It can be seen from the table that determining the diameter of the tray/plate column is an essential step in the design process. The diameter largely depends on the flooding correlation developed with the help of liquid flow parameter, F_{lv} and the capacity parameter, C_{sb}.[52] The flooding correlation developed by Fair and Matthews is shown in Figure 4.1.[46]

Table 4.2. Design specification check list for the over-all tray/plate column design

No.	Parameters to be determined
1	Column diameter
2	Number of trays
3	Tray spacing
4	Feed and drawoff locations
5	Operating temperatures and pressures
6	Materials of construction

*Adopted from Design of Equilibrium stage processes, Smith, 1963, Mc Graw Hill, New York.[52]

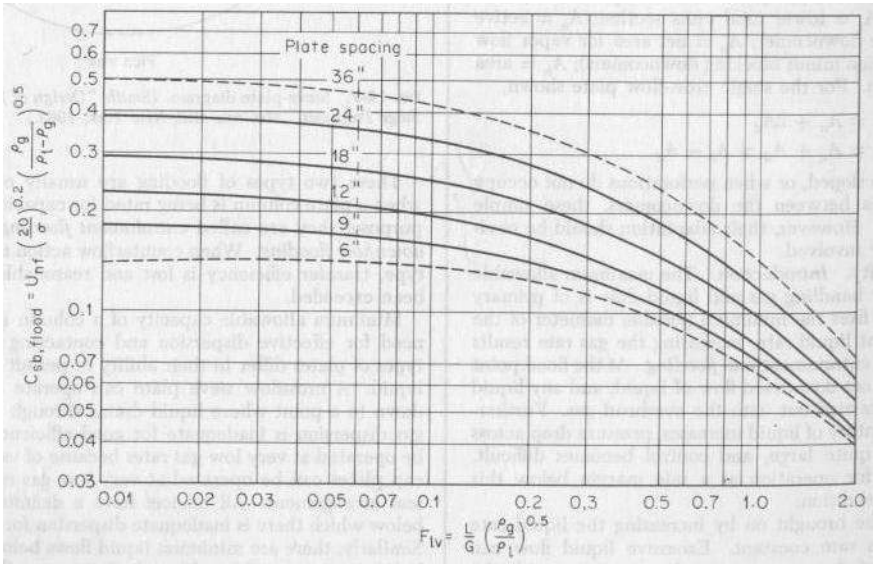

Figure 4.1. Flooding correlation for trays

The liquid flow parameter, F_{lv} accounts for the liquid flow effects resulting in flooding on the tray. It is the ratio of liquid to vapor kinetic energy effects.[52]

$$F_{lv} = \frac{Q_l}{Q_v}\sqrt{\frac{\rho_v}{\rho_L}} \tag{4.1}$$

The capacity parameter, C_{sb}, developed by Souders and Brown is given by the following expression:[52]

$$C_{sb} = V_{vf}\sqrt{\frac{\rho_v}{\rho_L - \rho_v}} \tag{4.2}$$

However the equation 4.2 is applicable only when the surface tension of the liquid is 20 dyne/cm. Hence the equation has been modified to equation 4.3 while applying it in liquids with surface tension that is different from 20dyne/cm

$$C_{sb(\sigma\neq 20)} = C_{sb(\sigma=20)}\left(\frac{\sigma}{20}\right)^{0.2} \tag{4.3}$$

With the help of the flooding correlation, the flooding vapor velocity V_{vf} is determined. The design vapor velocity is determined based on the percentage of flooding allowed.

$$V_v = \frac{V_{vf} \times (\%\, flooding)}{100} \tag{4.4}$$

The tower area, A_t and the tower diameter D_t are given by equation 4.5 and 4.6

$$A_t = \frac{Q_v}{V_v} \tag{4.5}$$

$$D_t = \sqrt{\frac{4A_t}{\Pi}} \tag{4.6}$$

The properties of ammonia-water solution are determined using the equations described in Appendix C. The design calculations for a sieve plate column are shown in greater detail in the Appendix D.

It was found that the tower diameter was in the range of 0.5 ft to 0.9 ft for the 5 KW ammonia/water combined cycle. The literature tells us that the application of the tray columns for tower diameters less than 2 ft will be very expensive. Moreover, the absorption process will be accompanied by heat rejection and hence cooling coils are to be incorporated on the plates. This will further increase the cost. For ammonia/water combined cycles with capacities in excess of 15-20 KW, the tray column becomes cost effective.

The main purpose of this study is to determine a configuration which will take into account both the absorption and the heat rejection process while keeping the cost of construction low. The use of a tray/plate column for the 5 KW ammonia/water combined cycle was not considered further as it will result in a large expenditure.

The bubble absorber developed by Kang et al. (1998)[32] was slightly modified and analyzed for the current situation. In the model developed by Kang et al. the liquid and the vapor flow in opposite directions. As the mass flow rate of the vapor is very low (372 lb/hr) compared to that of the weak solution (0.9389 kg/s), it might be difficult for the vapor to flow up while the weak solution is flowing down. Hence it was decided to analyze the absorber for co-current flow. The pressure drop for co-current flow will be much less compared to the pressure drop in a counter-current flow. The model for a bubble column involves a combined heat and mass transfer analysis. It considers the heat and mass transfer resistances not only in the liquid region but also in the vapor region. The outline of the model that was analyzed is shown in Figure 4.2

There is a significant mixing between the liquid and the vapor and hence in analyzing the absorption processes in the bubble mode, diffusion, concentration, mass and energy balances are considered in both the liquid and the vapor phase.

4.2 Design of a Bubble Absorber

4.2.1 Bubble Dynamics

Various correlations have been determined to find the bubble diameter. However the Bhavaraju's correlation (1978) is the most widely used one. It was shown that the liquid above the orifice can be divided into two regions, I and II.[2] Region I is characterized by large bubble sizes, lower hold-up, and non-uniform distribution of the

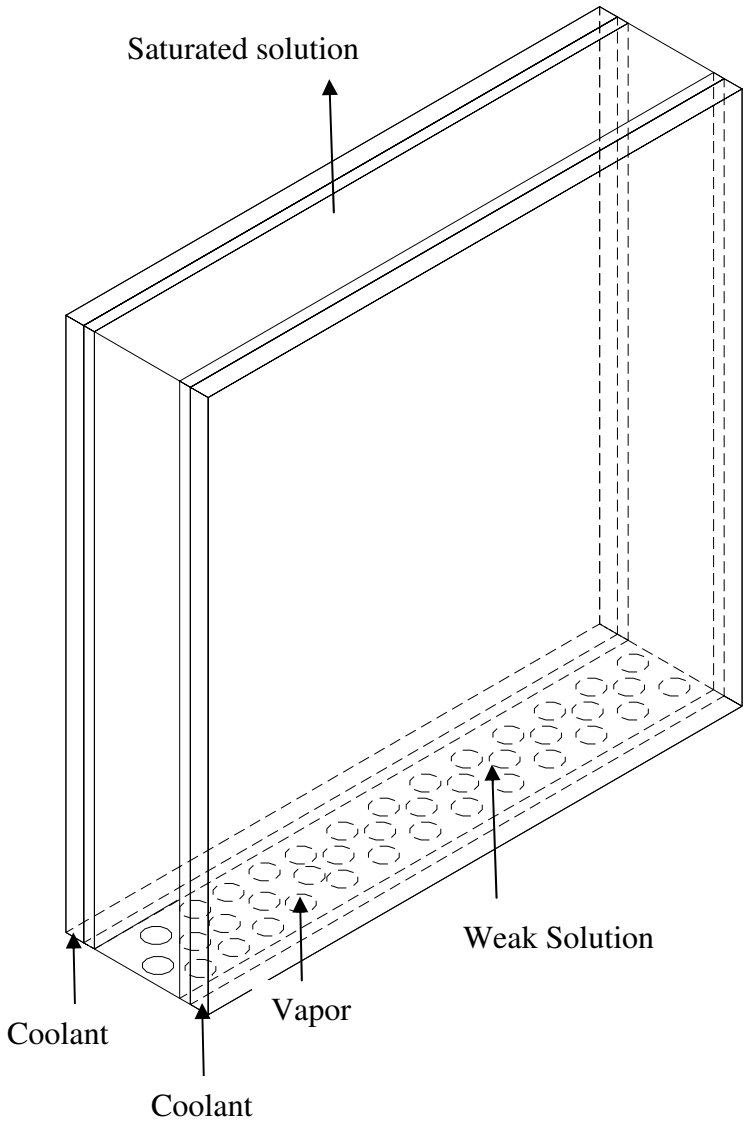

Figure 4.2. Model of the bubble absorber being analyzed

bubbles across the bottom of the absorber. The bubble properties in this region are determined by the bubble formation process at the orifice. In region II the bubble properties are determined by the bulk liquid motion. Bhavaraju et al.(1978) showed that the bubble break-up phenomenon occurs in region II and is related to liquid turbulence rather than the gas turbulence at the orifice.

Based on the gas flow rate, the bubble formation is divided into three regimes with very low gas rates, moderately high gas flow rates and very high gas rates. The expressions for the bubble diameter in these regions are tabulated in Table 4.3.

Table 4.3. Bhavaraju's correlations for bubble diameter

Very low gas rates	$Q_{v/o} < Q_t = \frac{\Pi g \Delta\rho}{108\mu_L}\left(\frac{6\sigma d_o}{g(\rho_L-\rho_g)}\right)^{4/3}$ for $\mathrm{Re}_B \le 1$ $= 0.32 g^{0.5}\left(\frac{6\sigma d_o}{g(\rho_L-\rho_g)}\right)^{5/6}$ for $\mathrm{Re}_B >> 1$	$d_B = \left(\frac{6\sigma d_o}{g(\rho_L-\rho_g)}\right)^{1/3}$ $\mathrm{Re}_B = \frac{\rho_L V_v d_B}{\mu_L}$
Moderately high gas rates	$Q_{v/o} > Q_t$ and $\mathrm{Re}_{ol} < 2000$ $\mathrm{Re}_{ol} = \frac{4\rho_L Q_{v/o}}{\Pi d_o \mu_L}$	$\frac{d_B}{d_o} = 3.23(\mathrm{Re}_{ol})^{-0.1}(Fr_o)^{0.21}$ $Fr_o = \frac{Q_{v/o}}{d_o^5 g}$
Very high gas rates	$\mathrm{Re}_{ol} > 2000$ 1. For $d_b < d_{bm}$ 2. $d_b > d_{bm} > d_{BE} = 0.0045$ m 3. For $d_{bm} < d_{BE} = 0.0045$ m	1. $\frac{d_B}{d_o} = 3.23(\mathrm{Re}_{ol})^{-0.1}(Fr_o)^{0.21}$ 2. $d_{bm} = 0.7\left(\frac{\sigma^{0.6}}{\left(\frac{P}{V}\right)^{0.4}\rho_L^{0.2}}\right)\left(\frac{\mu_{app}}{\mu_G}\right)^{0.1}$ $d_b = smallest(d_b, d_{bm})$ 3. $d_{BE} = 0.0045$ m

*Adopted from Bhavaraju, S.M., Russell, T.W.F., Blanch, H.W., 1978, "The Design of Gas Sparged Devices for Viscous Liquid Systems," AIChE Journal, Vol.24 (3), 454-466

The literature shows that the average vapor velocities expected in a bubble absorber are normally in the range of 0.01m/s to 0.7m/s. The orifice number and the orifice diameter are adjusted using equation 4.7 till the desired average vapor velocity is achieved (0.01m/s to 0.7m/s).

$$V_v = \frac{m_{abs}}{\rho_v A_o n_o} = \frac{m_{L(final)} - m_{L(initial)}}{\rho_v A_o n_o} \tag{4.7}$$

For the current model, the orifice diameter considered is 0.075m and the number of orifice is 900. The absolute vapor velocity is determined using equation 4.8.[2]

$$V_v = \frac{g\rho_L}{18\mu_L}\left(\frac{6\sigma d_o}{g(\rho_L - \rho_g)}\right)^{2/3} \quad \text{for } \mathrm{Re}_B < 1$$

$$= \left[\left(\frac{2\sigma}{\rho_L}\left(\frac{g(\rho_L - \rho_g)}{6\sigma d_o}\right)^{1/3}\right) + \left(\left(\frac{6\sigma d_o}{g(\rho_L - \rho_g)}\right)^{1/3}\frac{g}{2}\right)\right]^{1/2} \quad \text{for } \mathrm{Re}_B >> 1 \qquad (4.8)$$

After determining the vapor velocity, the equations in Table 4.3 are used to determine the bubble diameter.

4.2.2 Interfacial Area and Gas Hold-up

The liquid vapor interfacial area and gas hold-up play an important role in the mass transfer operation which determines the absorption rate. The interfacial area affects the volumetric mass transfer coefficient and the gas hold-up, ε_v influences the interfacial area.[32] The interfacial area is also influenced by the mean bubble diameter, d_B represented by equation 4.14. This correlation for the mean bubble diameter was given by Akita and Yoshida (1974).[25,36] Gas hold-up depends on the superficial vapor velocity and the various properties of the weak solution and the vapor. It was found that gas hold-up in aqueous electrolyte solutions is slightly larger than in pure liquids or non-electrolyte solutions. Hence a correction factor 'f' is used in the case of electrolyte solutions.

In order to calculate the gas hold-up, many correlations have been determined. However for the current application, the gas hold-up is calculated using the correlation given by Deckwer and Schumpe (1993). This correlation is shown in equation 4.9.

$$\varepsilon_v = \frac{V_v}{V_{sb}} \text{ if } V_v \le V_{trans}$$

$$= \frac{V_{trans}}{V_{sb}} + \frac{V_v - V_{trans}}{V_{lb}} \text{ if } V_v > V_{trans} \quad (4.9)$$

$$V_{sb} = \frac{2.25\sigma}{\mu_L}\left(\frac{\sigma^3 \rho_L}{g\mu_L^4}\right)^{-0.273}\left(\frac{\rho_L}{\rho_v}\right)^{0.03} \quad (4.10)$$

$$V_{bl} = \frac{\sigma}{\mu_l}\left\{\frac{V_{sb}\mu_L}{\sigma} + \left(2.4\left[\frac{\mu_L\left(V_v - V_{trans}\right)}{\sigma}\right]^{0.757}\left(\frac{\sigma^3\rho_L}{g\mu_L^4}\right)^{-0.077}\left(\frac{\rho_L}{\rho_v}\right)^{0.077}\right)\right\} \quad (4.11)$$

$$\frac{V_{trans}}{V_{sb}} = 0.5\exp\left(-193\rho_v^{-0.61}\mu_L^{0.5}\sigma^{0.11}\right) \quad (4.12)$$

The interfacial area for a spherical bubble is given by the equation (4.13).[36]

$$A_i = 6\frac{\varepsilon_v}{d_B} \quad (4.13)$$

$$\text{where } d_B = 26D_c\left(\frac{D_c^2\rho_L g}{\sigma}\right)^{-0.5}\left(\frac{D_c^3\rho_L^2 g}{\mu_L^2}\right)^{-0.12}\left(\frac{V_v}{\left(D_c g\right)^{0.5}}\right)^{-0.12} \quad (4.14)$$

However if ε_v<0.14, Akida and Yoshida presented the expression shown in equation 4.15[36] to estimate the interfacial area.

$$A_i = \frac{1}{3D_c}\left(\frac{gD_c^2\rho_L}{\sigma}\right)^{0.5}\left(\frac{gD_c^3\rho_L^2}{\mu_L^2}\right)^{0.1}\varepsilon_v^{1.13} \quad (4.15)$$

4.2.3 Mathematical Model using Control Volume Analysis

The flow of the vapor and the weak solution in the absorber has been mathematically modeled using a control volume analysis. The vapor bubbles and the weak ammonia solution flow upwards in a co-current direction while the coolant flows downwards on the outer wall as shown in Figure 4.3.

The following are the assumptions that were made to develop the model:

1. Absorption process is steady state
2. System pressure is constant.
3. There is no direct heat transfer between the vapor and the coolant
4. The bubble coalescence and breakup are negligible
5. The bubble size and velocity are constant locally along the absorber length
6. The bubble is assumed to be spherical and it is a particle with shape oscillations as it flows up the column.
7. Heat transfer to the coolant occurs through the bulk liquid
8. The latent heat difference at the interface includes the heat of reaction.

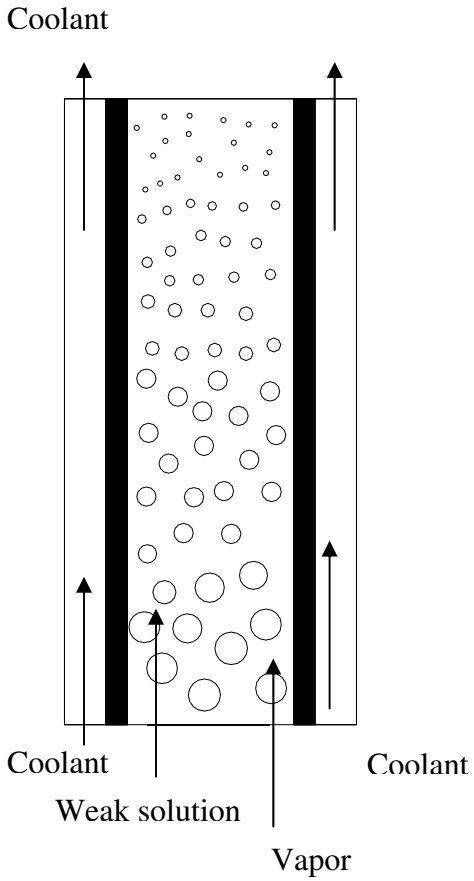

Figure 4.3. Front view of the bubble absorber

The control volume analysis involves solving the diffusion, concentration, mass and energy balance equations simultaneously.

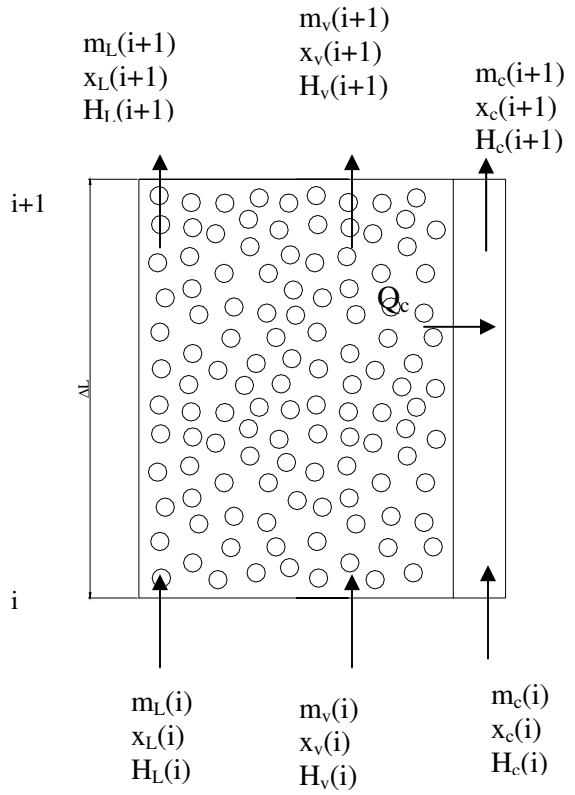

Figure 4.4. Control volume of a section of the absorber

The bubble is assumed to be a particle with shape oscillations whose natural frequency (Clift et. al) is given by equation 4.16.

$$f_N = \sqrt{\frac{48\sigma}{\Pi^2 d_B^3 \rho_L \left(2 + 3\frac{\rho_v}{\rho_L}\right)}} \tag{4.16}$$

The mass transfer coefficient of such a particle is calculated using equation 4.17 (Clift et. al)

$$K = 1.4\frac{A_s}{A_p}\sqrt{f_N \beta_p} \tag{4.17}$$

The heat and mass transfer analogy will be very useful when it is difficult to obtain any one of the heat and mass transfer coefficients. This is given in equation 4.18.

$$h = C_p K \left(\frac{Sc}{\Pr} \right)^{2/3} \tag{4.18}$$

There are a large number of correlations available for the heat and mass transfer coefficients in the liquid region. The correlations used for the current analysis are tabulated below.

Table 4.4. Heat and mass transfer coefficients

	Correlation	Comments
Liquid region	Akita and Yoshida (1974)[36] $K_L = \frac{0.5\beta_L}{d_B}\left(\frac{\mu_L}{\rho_L\beta_L}\right)^{0.5}\left(\frac{gd_B^3\rho_L^2}{\mu_L^2}\right)^{0.25}\left(\frac{gd_B^2\rho_L}{\sigma}\right)^{3/8}$	Valid for column diameters up to 60cm V_v<1500 m/hr Gas holdup up to 30%
	Deckwar et al (1980)[14] $St_L = 0.1\left(\mathrm{Re}_B\, Fr_L\, \Pr_L^2\right)^{-0.25}$ $Fr_L = \frac{V_v^2}{gd_B} \quad \Pr_L = \frac{\mu_L C_{p_L}}{k_L} \quad \mathrm{Re}_B = \frac{\rho_L V_v d_B}{\mu_L}$ $h_L = St_L \rho_L C_{p_L} V_v$	Valid only for V_v < 360m/hr
Vapor region	Clift et. al (1978)[5] $f_N = \sqrt{\frac{48\sigma}{\Pi^2 d_B^3 \rho_L \left(2 + 3\frac{\rho_v}{\rho_L}\right)}}$ $K_v = 1.4\frac{A_s}{A_p}\sqrt{f_N \beta_v}$	Assuming the bubble to be a particle with shape oscillations
	Mass transfer analogy $h_v = C_{p_v} K_v \left(\frac{Sc_v}{\Pr_v}\right)^{2/3}$ $\Pr_v = \frac{\mu_v C_{p_v}}{k_v} \quad Sc_v = \frac{\mu_v}{\rho_v \beta_v}$	

Diffusion Equation:

The mass transfer between the vapor and the weak solution is not only due to the mass transport between the bulk phases but also due to the diffusion of ammonia and water across the interface. The total molar flux absorbed/desorbed is given by equation 4.19 (Kang. et. al 1996).[31]

1. $$N_{NH_3} + N_{H_2O} = K_l \ln\left(\frac{z - x_L}{z - x_{Li}}\right) = K_v \ln\left(\frac{z - x_{vi}}{z - x_v}\right) \tag{4.19}$$

where

$$x_{Li} = f(T_i, P) \tag{4.20}$$

$$x_{vi} = f(T_i, P) \tag{4.21}$$

z is defined as the ratio of the ammonia molar flux absorbed/desorbed to the total molar flux absorbed/desorbed and is given by equation 4.22.

$$z = \frac{N_{NH_3}}{N_{NH_3} + N_{H_2O}} \tag{4.22}$$

If $N > 0$, it shows that the mass is being absorbed from the vapor into the weak solution. With the help of the control volume shown in Figure 4.4, the mass and concentration balance are given by the following equations:

Mass Balance Equation:

1. Mass balance for the vapor phase in the control volume

$$m_v(i+1) = m_v(i) - \left(N_{NH_3} + N_{H_2O}\right)\Delta A_m \tag{4.23}$$

2. Mass balance for the liquid phase in the control volume

$$m_L(i+1) = m_L(i) + \left(N_{NH_3} + N_{H_2O}\right)\Delta A_m \tag{4.24}$$

where ΔA_m is the mass transfer area between the liquid and the vapor phase and it is given by the following expression

$$\Delta A_m = A_i A_c \Delta L \tag{4.25}$$

Concentration balance Equation:

1. Concentration balance for the vapor phase in the control volume

$$m_v(i+1)x_v(i+1) = m_v(i)x_v(i) - z\left(N_{NH_3} + N_{H_2O}\right)\Delta A_m \tag{4.26}$$

2. Concentration balance for the liquid phase in the control volume

$$m_L(i+1)x_L(i+1) = m_L(i)x_L(i) + z\left(N_{NH_3} + N_{H_2O}\right)\Delta A_m \tag{4.27}$$

Energy Balance Equation:

In general heat transfer due to convection occurs due to temperature difference between two surfaces. However the heat transfer between the vapor and the weak solution occurs not only due to convection but also due to the sensible heat load. If this heat transfer is accompanied by mass transfer at the inter phase then an additional amount of heat will be added due to the heat capacity of the mass. Hence the convective heat transfer coefficient h is modified in order to account for this heat as a result of the mass transfer. The modified convective heat transfer coefficient is given by equation 4.28.[61, 19]

$$h_{mj} = h_j \frac{c_j}{1 - \exp(-c_j)} \tag{4.28}$$

$$c_j = \frac{N_{NH_3} C_{pNH_3} + N_{H_2O} C_{pH_2O}}{h_j} \tag{4.29}$$

where h_{mj} is the modified heat transfer coefficient and 'j' stands for either the vapor phase or the liquid phase.

The sensible heat of the vapor that is transferred to interface is given by equation 4.30.

$$Q_{senv} = h_{m\,v}\left(T_v - T_i\right)\Delta A_m \tag{4.30}$$

$$c_v = \frac{N_{NH_3} C_{pNH_3 v} + N_{H_2O} C_{pH_2Ov}}{h_v} \tag{4.31}$$

The sensible heat of the weak solution transferred to the interface is given by Q_{senL}

$$Q_{senL} = h_{m\,L}\left(T_i - T_L\right)\Delta A_m \tag{4.32}$$

$$c_L = \frac{N_{NH_3} C_{pNH_3 L} + N_{H_2O} C_{pH_2OL}}{h_L} \tag{4.33}$$

1. Energy balance for the vapor phase in the control volume

$$m_v(i+1)H_v(i+1) = m_v(i)H_v(i) - Q_{senv} - dm_{NH_3} H_{NH_3 vi} - dm_{H_2O} H_{H_2Ovi} \text{ [§]} \tag{4.34}$$

2. Energy balance for the liquid phase in the control volume

$$Q_c + m_L(i+1)H_L(i+1) = m_L(i)H_L(i) + Q_{senL} + dm_{NH_3} H_{NH_3Li} + dm_{H_2O} H_{H_2OLi} \tag{4.35}$$

3. Energy balance at the interface

$$Q_{senL} + dm_{NH_3} H_{NH_3Li} + dm_{H_2O} H_{H_2OLi} = Q_{senv} + dm_{NH_3} H_{NH_3vi} + dm_{H_2O} H_{H_2Ovi} \tag{4.36}$$

The heat is transferred to the coolant through the liquid phase. The heat transfer to the coolant Q_c can be found in three different ways as shown below.

1. Energy balance in the control volume

$$Q_c = \left(m_L(i)H_L(i) + m_v(i)H_v(i)\right) - \left(m_L(i+1)H_L(i+1) + m_v(i+1)H_v(i+1)\right) \tag{4.37}$$

2. Energy balance in the coolant

$$Q_c = m_c(i+1)H_c(i+1) - m_c(i)H_c(i) \tag{4.38}$$

---

§ $N = \dfrac{dm}{M}$

dm is the mass flux absorbed/desorbed and N is the molar flux absorbed/desorbed

3. Energy balance between the liquid and the coolant interface

$$Q_c = UA_{c/s}\left(T_L - T_c\right) \tag{4.39}$$

where

$$\frac{1}{U} = \frac{1}{h_c} + R_{wall} + \frac{1}{h_l} \tag{4.40}$$

The design conditions given are shown in Figure 4.5. The analysis requires the thermodynamic and transport properties of ammonia and water mixtures. The empirical correlations used to find the thermodynamic properties are shown in Appendix C.

m_L = 7824.68 lb/hr = 0.98591 kg/s
m_v = 0 lb/hr
x_L = 0.3996
H_L = -5 Btu/lb = 11.63 KJ/kg
T_L = 100°F = 310.78 °K

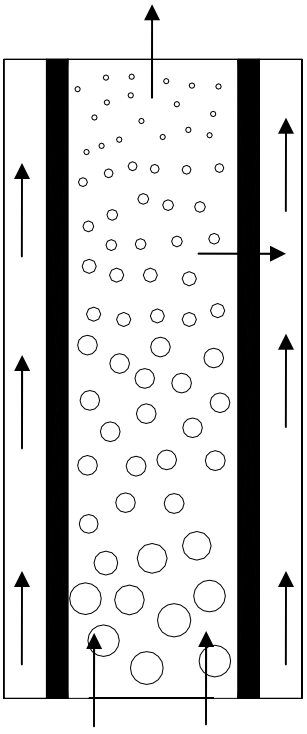

m_L= 7452.31 lb/hr=0.9389 kg/s
x_L = 0.3646
T_L = 114°F = 318.56 °K
H_L = 12 Btu/lb = 27.91 KJ/kg

m_v = 372.37 lb/hr = 0.0469 kg/s
x_v = 0.999
T_v = 85°F = 302.44 °K
H_v = 656.1 Btu/lb = 1526.08 KJ/kg

Figure 4.5. Design conditions

4.2.4 Numerical Method used to Solve the Diffusion, Mass, Concentration and Energy Balance Equations

The absorber is divided into differential elements and the analysis is carried over the individual elements. An element of length ΔL is considered as shown in Figure 4.4 The convergence criterion assumed is 10^{-5}. The steps involved in solving the equations are shown in Figure 4.6.

4.2.5 Analysis

The model was simulated using Matlab. However, there was an abrupt jump in the values of 'z' and the effect was carried over to the other parameters. This typical phenomena needs to be looked into at a greater detail by experimental analysis. This will also help in confirming the application of the correlations used for the current situation. As the reason for the discontinuity in 'z' has not been analyzed, the current study did not concentrate on the coolant details. More details about the results are discussed in Appendix E.

A detailed comparison of the five different configurations that have been studied is shown in Table 4.5.

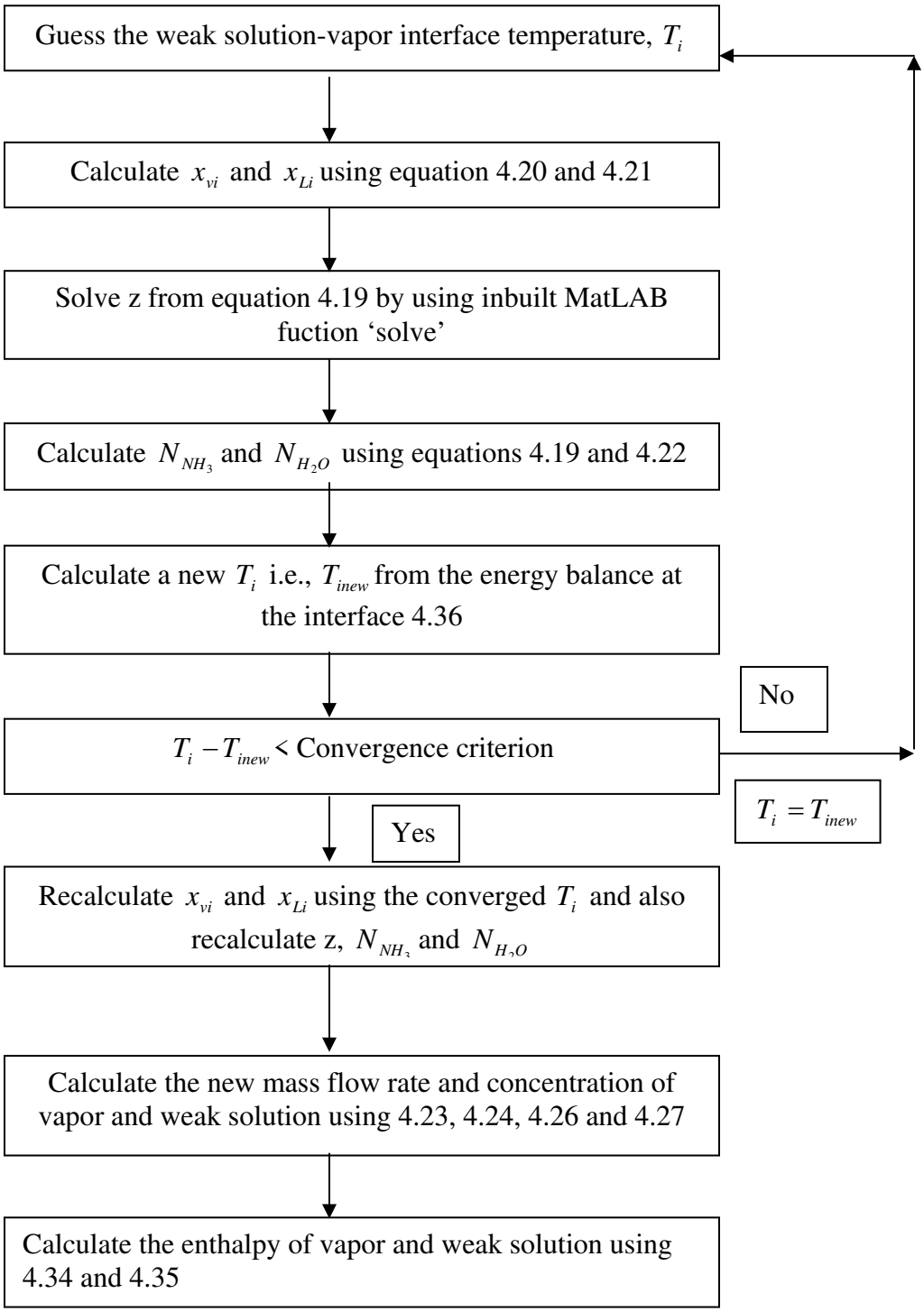

Figure 4.6. Steps involved in the numerical analysis[**]

[**] This does not include the coolant flow iterations

Table 4.5. Different configurations of the absorber that were studied as a part of the analysis

	Falling film	Spray absorber	Bubble absorber	Packed column absorber	Tray absorber
Mass transfer	Mass transfer dominates the absorption process. Low mass transfer rates.	High mass transfer rate.	High mass transfer rate as a large volume of the vapor comes in contact with the liquid.	Mass transfer is high.	Mass transfer rates are high.
Interfacial area	The interfacial area between the vapor and the liquid is low.	High interfacial area as the liquid is sprayed into a chamber containing vapor.	The interfacial area between the vapor and the liquid is high.	The packing enhances the interfacial area between the liquid and the vapor.	A large volume of the vapor comes in contact with the liquid solution as the vapor is sent out in the form of bubbles.
Applicability to the absorber that will be incorporated in the 5KW ammonia/water combined cycle	The vapor flow rate is very low at the inlet of the absorber. Hence the chances of absorption will be very less as the contact area between the weak solution and the vapor will be low.	It might be a good configuration to consider. However if the nozzle that is used to spray the liquid is not appropriately chosen then it results in higher pumping power and higher costs.	This might be a very good option considering the mass transfer point of view.	Considering the increased interfacial area between the liquid and the vapor, this seems to be a good option.	The vapor flow rate is very low at the inlet of the absorber. Hence this might be a very good option considering the mass transfer point of view.

Table 4.5 continued

	Falling film	Spray absorber	Bubble absorber	Packed column absorber	Tray absorber
Removal of heat/ Heat transfer.	Cooling coils can be incorporated easily.	Effective heat rejection as the heat is rejected in a separate chamber.	Heat can be rejected to a coolant easily and the contact area between the liquid and the coolant is also high for effective heat transfer.	Incorporating cooling coils is difficult.	Incorporating cooling coils is easier than packed column absorbers.
Applicability to the absorber that will be incorporated in the 5KW ammonia/water combined cycle	Removal of heat will be easy as it is easy to incorporate cooling coils. However the problems of wettability result in low heat transfer.	Might be a good configuration if the nozzle picked is the right one.	Removal of heat will be easy.	Removal of heat of condensation is very important for the absorption to continue. The bulk liquid temperature at the inlet of the absorber is as high as 318.56^{o}K.Hence removal of heat plays an important role. Multi-stage absorption increases the rate of absorption but the cost is also high.	Heat removal is easier than packed columns. However the calculations show that the column diameter of the absorber that will be used in the combined cycle is small (<2feet) and tray columns with small diameters will be cost inefficient from the manufacturing point of view.

Table 4.5 continued

	Falling film	Spray absorber	Bubble absorber	Packed column absorber	Tray absorber
Wettability	They have high wettability problems as the contact area between the liquid and the vapor is very low.	Wettability problems arise due to improper distribution of the liquid through the nozzles.	There will no problems of wettability as there is a large volume of vapor that is coming in contact with the liquid.	Application of packed columns requires a minimum liquid load given by equation 3.1. If this load is not satisfied, it leads to wettability problems.	Wettability problems can be resolved by balancing the down flow capacity of the liquid and the allowed entrainment of liquid along with the gas.
Applicability to the absorber that will be incorporated in the 5KW ammonia/water combined cycle	The vapor flow rate is very low and hence the interfacial area between the liquid and the vapor will not be enough for the absorption process to take place efficiently.	The vapor flow rate is low in the 5KW combined cycle. If the nozzle chosen is not appropriate, then it will lead to non-uniform distribution of liquid and as a result there would not only be inefficient absorption but also the cost will be higher.	As there are no wettability problems, this will be a good design.	The liquid flow rate at the inlet of the absorber satisfies this condition. Hence there will be no wettability problems.	
Pressure drop	Low compared to tray and packed columns.	High if the wrong nozzle is chosen.	Low compared to tray and packed columns	Low compared to tray column absorbers.	High

Table 4.5 continued

	Falling film	Spray absorber	Bubble absorber	Packed column absorber	Tray absorber
Summary comments	Not a very good design for the current design conditions.	Might be a good choice if the appropriate nozzle is chosen. This design needs to be explored to a greater extent.	Considering the heat transfer, mass transfer and cost , this seems to be a better choice when compared to all other absorbers. However the modeling of the process is difficult because of the complex bubble dynamics involved. Hence the results need to be analyzed experimentally.	The mass flow rate of the vapor is very low in the 5 KW ammonia/water combined cycle.. The heat of condensation needs to be removed for all the vapor to be absorbed. Incorporating cooling coils in a packed column is very difficult. Hence this design is not advisable.	From the viewpoint of heat and mass transfer this seems to be applicable to the current situation. However the design calculations (in Appendix E) show that the tower diameter for the 5 KW ammonia/water combined cycle is less than 2ft and hence this will turn out to be very expensive and is not applicable.

CHAPTER 5
CONCLUSIONS

This thesis was a study of the absorber operations for the 5KW ammonia/water combined cycle. The required design conditions had two important characteristics viz.,

1. The amount of ammonia to be absorbed from the weak solution can be as low as 3%.
2. The ratio of the mass flow rate of the weak solution to the vapor flow rate is very high (20:1).

As the vapor flow rate is very low, the entire vapor should come in contact with the weak solution in order to achieve an increase in the mass fraction of the ammonia in this solution. However for the absorption process to be continuous there should be a provision for the removal of the heat of condensation.

A detailed comparison of the five different configurations of the absorber shown in Table 4.5 lead to the following conclusions:

1. Considering the theoretical analysis, the bubble absorber is the best choice for the 5 KW ammonia/water combined cycle.
2. The construction cost of the bubble absorber should be much less when compared to other configurations.

The results from the simulations lead to the following conclusions:

1. The ratio of the length of the absorber to the width was found to be 9:1 and the height of the absorber varied from 1.7m to 2.2m depending on the inlet bulk liquid temperature.

2. A rapid change in the properties was noticed at a height of 0.2m from the bottom. This is the height at which the absorption process starts.
3. The height of the absorber reduced by 20% when the inlet weak solution was sub-cooled from 318.56^{o}K to 300^{o}K.
4. The complexity of the bubble dynamics and the rapid change in the properties suggest that the model of the bubble absorber needs to be verified experimentally.

CHAPTER 6
RECOMMENDATIONS

The absorber operations for the 5KW ammonia/water combined cycle have been analyzed. For the required design conditions, the bubble absorber seemed to be the best fit. However the model for this absorber was difficult to develop due to the complex bubble dynamics. The analysis was carried out by solving the diffusion, concentration, mass and energy balance equations simultaneously using MatLAB. The results showed an abrupt change in the data at a height where the absorption starts. The reason for this sudden change needs to be observed in greater detail. Also the results (in Appendix E) show that the absorber height decreased when the bulk temperature of the liquid is reduced from 318.56^{o}K to 300^{o}K.

The behavior of the model under various inlet conditions has to be observed with additional simulations. More analysis needs to be done on the bubble dynamics. The modeling involves the application of various correlations along with the assumption that the difference in the enthalpy of the liquid and the vapor at the interface includes the heat of reaction. The authenticity of applying these correlations and assumptions to the current situation needs to be verified experimentally.

As the construction of the absorber might involve a large amount of financial investment, as a first step, it is recommended to run more simulations. The current model involves co-current flow between the vapor, weak solution and the coolant. However it is advisable to incorporate counter-current flow not only between the weak solution and the coolant but also between the weak solution and the vapor. The heat transfer and mass

transfer coefficients in a counter-current flow are very large and hence this might improve the absorption process and reduce the size of the absorber.

APPENDIX A
AMMONIA TOXICITY

The toxic nature of ammonia is detailed in Table A.1, giving exposure limits and the corresponding responses exhibited by humans.

Table A.1. Ammonia exposure limits.

Exposure (ppm)	Effects
0-5	Smell hardly detectable.
5-20	Human nose starts to detect.
25	TLV-TWA (Threshold Limit Value – Time Weighted Average, 8 h)
35	STEL (Short Term Exposure Limit – 15 min).
150-200	Eyes affected to limited extent after about 1 min exposure. Breathing not affected.
500	IDLH (Immediately Dangerous to Life and Health, per NIOSH).
600	Eyes streaming in about 30 s exposure.
700	Tears to eyes in seconds. Still breathable.
1000	Eyes streamed instantly and vision impaired, but not lost. Breathing intolerable to most participants. Skin irritation to most participants.
1500	Instant reaction is to get out.

Adopted from Tamm, Gunnar Olavi., 2003, "Experimental Investigation of an Ammonia-Based Combined Power and Cooling Cycle," Ph.D. Dissertation, University of Florida.

APPENDIX B

CRITERIA TO USE TRAY COLUMNS AND COMPARISION BETWEEN BUBBLE, SIEVE, VALVE AND PACKED COLUMNS

Table B.1. Criteria for use of tray or packed columns

Criteria of Selection	Tray Column	Packed Column
Tower diameter	Generally employed in large diameter towers (> than 1m i.e., 3.281 ft.)	Small diameter (<0.7m i.e., 2.29 ft) With structured packings it can be used for large diameter towers also
Downcomers	Several are necessary	No downcomers necessary
Gas load	Should be in a narrow range (Valve trays allow greater operational flexibility)	Flexible range, it can be operated over a wide range
Liquid load	Can be varied over a very wide range . They can be operated in vacuum operations	Minimum liquid load. This excludes their use in vacuum operation
Result of low liquid load	Operates very efficiently even for low liquid loads	Inefficient for low liquid loads
Pressure drop	High 7mbar per equilibrium stage	Small 0.5 mbar per equilibrium stage
Heat exchanger coils	Can be incorporated easily	Difficult to incorporate cooling coils
Impurities in liquid	These are insensitive to liquid impurities	They are not suitable with liquid with impurities and liquids that tend to crystallize
Danger of decomposition of thermally unstable substances	Is high coz of liquid hold-up in the tray and in the downcomer	Is low coz liquid hold-up is very low
Foaming	High	Less sensitive than tray columns

Table B.2. Comparision between bubble cap, sieve, valve and packed columns

Criteria of comparison	Bubble Cap column	Sieve Tray column	Valve plate column	Packed columns
Method of Manufacture	Complicated	Easy to manufacture	Easier than bubble cap columns	Easier than tray columns
Cost to manufacture	Expensive	Inexpensive	20% more expensive than sieve tray columns	For columns < 2ft diameter, packings are cheaper than trays
Efficiency	Operates satisfactorily. Efficiency same or less than sieve trays	Efficiency good	Efficiency remains high even when gas rate drops	Low liquid rates lead to incomplete wetting and this decreases efficiency Can't handle high liquid rates
Flexibility	Quite flexible	Not extremely flexible	More flexible when feed rate varies	Less flexible than tray columns
Problems with fouling and solid particles in the liquid	Problems with coking, polymer formation or high fouling mixture	Good in fouling applications, good when solids are present	More likely to foul or plug	If solids are present in liquid or gas, plate columns can be designed to permit easier cleaning
Hold-up liquid	Hold-up liquid is high and can lead to the decomposition of thermally unstable compounds			Hold-up liquid very less
Incorporation of cooling Coils	Cooling coils can be incorporated more readily than packed columns			Incorporation of cooling coils is difficult
Operating range	Operating range is higher than packed columns			Narrow operating range

APPENDIX C
THERMODYNAMIC AND TRANSPORT PROPERTIES OF AMMONIA-WATER MIXTURE

C.1 Thermodynamic Properties of Ammonia/Water Mixture

The equations used to find the thermodynamics properties of ammonia/water mixture are based on the correlations given by Ziegler and Trepp.[65] Xu and Goswami developed a method (1999) which combined the Gibb's free energy method for the mixture properties and the bubble and dew point temperature equations for the phase equilibrium. . These correlations are valid in the range of 230-600 K for the temperature and 0.2-110 bar for pressure. This appendix includes the calculation of enthalpy and specific volume. The Gibb's free energy of a pure component is given by

$$G = H_o - TS_o + \int_{T_o}^{T} C_p dT + \int_{P_o}^{P} v dP - T\int_{T_o}^{T} \frac{C_p}{T} dT \qquad \text{(C.1)}$$

The subscript 'o' is used in context with the reference state. The following relations were assumed by Ziegler and Trepp .

Table C.1. Expressions for specific heat and specific volume

For liquid phase	For vapor phase
$v_L = a_1 + a_2 P + a_3 T + a_4 T^2$	$v_v = \frac{RT}{P} + c_1 + \frac{c_2}{T^3} + \frac{c_3}{T^{11}} + \frac{c_4 P^2}{T^{11}}$
$C_{P,L} = b_1 + b_2 T + b_3 T^2$	$C_{P,v} = d_1 + d_2 T + d_3 T^2$

The application of these relations in equation C.1 results in equation C.2 and C.3.

For liquid phase:

$$G_{r,L} = H_{r,o,L} - TS_{r,o,L} + B_1\left(T_r - T_{r,0}\right) + \frac{B_2}{2}\left(T_r^2 - T_{r,o}^2\right) + \frac{B_3}{3}\left(T_r^3 - T_{r,o}^3\right)$$
$$- B_1 T_r \ln\left(\frac{T_r}{T_{r,o}}\right) - B_2 T_r\left(T_r - T_{r,o}\right) - \frac{B_3}{2} T_r\left(T_r^2 - T_{r,o}^2\right)$$
$$+ \left(A_1 + A_3 T_r + A_4 T_r^2\right)\left(P_r - P_{r,o}\right) + \frac{A_2}{2}\left(P_r^2 - P_{r,o}^2\right) \qquad \text{(C.2)}$$

For vapor phase:

$$G_{r,v} = H_{r,o,v} - TS_{r,o,v} + D_1\left(T_r - T_{r,0}\right) + \frac{D_2}{2}\left(T_r^2 - T_{r,o}^2\right) + \frac{D_3}{3}\left(T_r^3 - T_{r,o}^3\right)$$
$$- D_1 T_r \ln\left(\frac{T_r}{T_{r,o}}\right) - D_2 T_r\left(T_r - T_{r,o}\right) - \frac{D_3}{2} T_r\left(T_r^2 - T_{r,o}^2\right) + T_r \ln\left(\frac{P_r}{P_{r,o}}\right)$$
$$+ C_2\left(\frac{P_r}{T_r^3} - 4\frac{P_{r,o}}{T_{r,o}^3} + 3\frac{P_{r,o}T_r}{T_{r,o}^4}\right) + C_3\left(\frac{P_r}{T_r^{11}} - 12\frac{P_{r,o}}{T_{r,o}^{11}} + 11\frac{P_{r,o}T_r}{T_{r,o}^{12}}\right)$$
$$+ C_1\left(P_r - P_{r,o}\right) + \frac{C_4}{3}\left(\frac{P_r^3}{T_r^{11}} - 12\frac{P_{r,o}^3}{T_{r,o}^{11}} + 11\frac{P_{r,o}^3 T_r}{T_{r,o}^{12}}\right) \qquad \text{(C.3)}$$

Reference state: $T_B = 100K \quad P_B = 10bar$

The thermodynamic properties in the reduced form for the above reference states are:

$$T_r = \frac{T}{T_B} \qquad \text{(C.4)}$$

$$P_r = \frac{P}{P_B} \qquad \text{(C.5)}$$

$$G_r = \frac{MG}{RT_B} \qquad \text{(C.6)}$$

$$H_r = \frac{MH}{RT_B} \qquad \text{(C.7)}$$

$$V_r = \frac{MVP_B}{RT_B} \qquad \text{(C.8)}$$

Table C.2. Coefficients of Gibbs energy relation

Coefficient	Ammonia	Water
A_1	3.971423×10^{-2}	2.8748796×10^{-2}
A_2	-1.790557×10^{-5}	-1.016665×10^{-5}
A_3	-1.308905×10^{-2}	-4.452025×10^{-3}
A_4	3.752836×10^{-3}	8.389246×10^{-4}
B_1	1.634519×10	1.214557×10
B_2	-6.50812	-1.8987
B_3	1.448937	2.911966×10^{-1}
C_1	-1.049377×10^{-2}	2.136131×10^{-2}
C_2	-8.28822	-3.169291×10
C_3	-6.647257×10^{2}	-4.634611×10^{4}
C_4	-3.04532×10^{3}	0
D_1	3.673647	4.01917
D_2	9.989629×10^{-2}	-5.175550×10^{-2}
D_3	3.617622×10^{-2}	1.951939×10^{-2}
$H_{r,o,L}$	4.878576	21.82114
$H_{r,o,v}$	26.46887	60.96506
$T_{r,o}$	3.2252	5.0705
$P_{r,o}$	2.0	3.0

Maxwell's relations are used to obtain the thermodynamic properties of pure fluids. The Gibb's free energy function is substituted in these equations.

$$H = -\frac{RT_B T_r^2}{M}\left(\frac{\partial}{\partial T_r}\left(\frac{G_r}{T_r}\right)\right)_{P_r} \tag{C.9}$$

$$v = \frac{RT_B}{MP_B}\left(\frac{\partial G_r}{\partial P_r}\right)_{T_r} \tag{C.10}$$

However the thermodynamics properties of a mixture deviate considerably from the ideal mixing behavior. For the liquid mixture, the deviation is accounted by the Gibbs excess energy, G^E.

$$G_r^E = (1-\tilde{x})\left\{F_1 + F_2(2\tilde{x}-1) + F_3(2\tilde{x}-1)^2\right\} \tag{C.11}$$

Where F_1, F_2, F_3 are given by

$$F_1 = E_1 + E_2 P_r + (E_3 + E_4 P_r)T_r + \frac{E_5}{T_r} + \frac{E_6}{T_r^2} \tag{C.12}$$

$$F_2 = E_7 + E_8 P_r + (E_9 + E_{10} P_r)T_r + \frac{E_{11}}{T_r} + \frac{E_{12}}{T_r^2} \tag{C.13}$$

$$F_3 = E_{13} + E_{14} P_r + \frac{E_{15}}{T_r} + \frac{E_{16}}{T_r^2} \tag{C.14}$$

Table C.3. Coefficients of Gibbs excess energy relation

E_1	-41.733398	E_9	0.387983
E_2	0.02414	E_{10}	-0.004772
E_3	6.702285	E_{11}	-4.648107
E_4	-0.011475	E_{12}	0.836376
E_5	63.608967	E_{13}	-3.553627
E_6	-62.490768	E_{14}	0.000904
E_7	1.761064	E_{15}	24.361723
E_8	0.008626	E_{16}	-20.736547

Hence the liquid mixture properties can be obtained by the following equations:

$$H_{awL}M_{awL} = \tilde{x}H_{NH_3L}M_{NH_3} + (1-\tilde{x})H_{H_2OL}M_{H_2O} + H^E M_{awL} \quad \text{(C.15)}$$

$$\nu_{awL}M_{awL} = \tilde{x}\,\nu_{NH_3L}M_{NH_3} + (1-\tilde{x})\nu_{H_2OL}M_{H_2O} + \nu^E M_{awL} \quad \text{(C.16)}$$

C.2 Transport Properties of Ammonia/Water Mixture

The transport properties like diffusivity, thermal conductivity and viscosity affect the mass transfer in an absorber. Thermal conductivity and viscosity data for the liquid and the vapor phases have been correlated by Yaws (1995). The estimated values were obtained by using Chapman-Enskog and Reichenberg techniques.[19]

For liquid phase:

$$\eta_{H_2OL} = -0.2758 + (4.612\times10^{-3})T - (5.5391\times10^{-6})T^2 \quad \text{(C.17)}$$

$$\eta_{NH_3L} = 1.1606 - (2.284\times10^{-3})T + (3.1245\times10^{-18})T^2 \quad \text{(C.18)}$$

$$\log_{10}\mu_{H_2OL} = -10.2158 + \left(\frac{1.7925\times10^3}{T}\right) + (1.773\times10^{-2})T - (1.2631\times10^{-5})T^2 \quad \text{(C.19)}$$

$$\log_{10}\mu_{NH_3L} = -8.591 + \left(\frac{8.764\times10^2}{T}\right) + (2.681\times10^{-2})T - (3.612\times10^{-5})T^2 \quad \text{(C.20)}$$

For vapor phase:

$$\eta_{H_2Ov} = 0.00053 + (4.7093\times10^{-5})T + (4.9551\times10^{-7})T^2 \quad \text{(C.21)}$$

$$\eta_{NH_3v} = 0.00457 + (2.3239\times10^{-5})T + (1.481\times10^{-7})T^2 \quad \text{(C.22)}$$

$$\mu_{H_2Ov} = -36.8255 + (4.2916\times10^{-1})T - (1.624\times10^{-5})T^2 \quad \text{(C.23)}$$

$$\mu_{NH_3v} = -7.8737 + (3.6745\times10^{-1})T - (4.4729\times10^{-6})T^2 \quad \text{(C.24)}$$

In the above relations, the gas viscosity is in micropoise, liquid viscosity is in centipoise, thermal conductivity is in W/mK and temperature is in ^{o}K. The following

correlations were used to find the diffusion coefficient and viscosity of ammonia/water liquid mixture (Frank et al., 1996, as cited in Goel[19]) Both the properties are in SI units. The dissociation of ammonia is large at low ammonia mass fractions and hence the correlations are not applicable to pure water.

$$\mu_{awL} = \left\{\left(0.67 + 0.78\tilde{x}\right)\times 10^{-6}\right\} e^{17900/RT} \tag{C.25}$$

$$D_{awL} = \left\{\left(1.65 + 2.47\tilde{x}\right)\times 10^{-6}\right\} e^{-16600/RT} \tag{C.26}$$

To determine the diffusion coefficient of the binary gaseous mixture, the Fuller et. Al correlation is recommended.

$$D_{awv} = \frac{0.00100T^{1.75}\sqrt{\left[1/M_1\right]+\left[1/M_2\right]}}{P\left[\left(\sum v\right)_1^{1/3} + \left(\sum v\right)_2^{1/3}\right]^2} \tag{C.27}$$

where M_1 and M_2 are the molecular weights of ammonia and water.

$\left(\sum v\right)$ is sum of the atomic diffusion volume of the basic elements.

$$\left(\sum v\right)_{H_2O} = 12.7 \tag{C.28}$$

$$\left(\sum v\right)_{NH_3} = 14.9 \tag{C.29}$$

The method derived by Jamieson et al., 1975, (as cited in Goel[19]), is used to estimate the thermal conductivities of binary liquid mixtures.

$$\eta_{awL} = x_1\eta_1 + x_2\eta_2 - \alpha\left(\eta_2 - \eta_1\right)\left(1 - x_2^{1/2}\right)x_2 \tag{C.30}$$

Where x_1, x_2 are the mass fraction and η_1 and η_2 are the thermal conductivities of the component 1 and 2. The components are to be chosen in such a way that $\eta_1 > \eta_2$.

α is the characteristic parameter of the binary mixture and it can be taken as unity if the experimental data are unavailable for regression analysis.

APPENDIX D
DESIGN CALCULATIONS OF A TRAY COLUMN ABSORBER (SIEVE PLATE ABSORBER)

The design calculations of the sieve plate absorber based on the design conditions mentioned in Chapter 4 are shown in Table D.1. The properties of ammonia/water are calculated at $112^{o}F/318^{o}K$ using the equations described in Appendix C. These calculations are done only for one stage. However the tray spacing has been varied from 6" to 36" in order to see how it affects the tower diameter. While the other parameters are kept constant, an increase in the tray spacing results in smaller tower diameter. But care should be taken to monitor the vapor and the liquid flow rate as the spacing is increased. Otherwise it might result in greater pressure loss, entrainment and weeping. As the vapor flow rate is much less compared to the liquid flow rate, the percent flooding/entrainment is considered to be as high as 80%. The percent flooding has been varied from 10-80% and in all the cases the tower diameter was less than 2ft. However, increasing the vapor flow rate while keeping the liquid flow rate constant resulted in an increase in the tower diameter. Hence the tray column absorbers are suitable for higher flow rates of liquid and vapor. The vapor flow rate at the inlet of the absorber of the 5 KW ammonia/water combined cycle is very low compared with the liquid low rate. As a result the tower diameter was found to be less than 2 feet. Considering the cost of manufacturing, it is not advisable to use a tray column absorber for tower diameters less than 2 feet. Hence this design was not explored any further for the 5KW ammonia/water combined cycle.

Table D.1. Design calculations for a tray column absorber

Q_l	Q_v	Q_{vfps}
7452.3100	372.3700	0.9090

ρ_v	ρ_L	F_{lv}	$\sqrt{\frac{\rho_v}{\rho_L - \rho_v}}$	σ	$\%\ flooding$
0.1138	53.6115	0.9220	21.6827	59.4600	80

$Tray\ spacing$	C_{sb}	$C_{sb(\sigma \neq 20)}$	V_{vf}	V_v	A_t	$D_t\,(feet)$	$D_t\,(m)$
6	0.0700	0.0870	1.8873	1.5099	0.6020	0.8755	0.2669
9	0.0800	0.0995	2.1570	1.7256	0.5268	0.8190	0.2496
12	0.0900	0.1119	2.4266	1.9413	0.4682	0.7721	0.2353
18	0.1100	0.1368	2.9658	2.3727	0.3831	0.6984	0.2129
24	0.1500	0.1865	4.0443	3.2354	0.2809	0.5981	0.1823
36	0.1800	0.2238	4.8532	3.8825	0.2341	0.5460	0.1664

Q_l lb/hr

Q_v lb/hr

Q_{vfps} cfs

ρ_v lb/ft^3

ρ_L lb/ft^3

σ [††] dyne/cm

V_v fps

[††] For the correlation to be valid the surface tension, σ is in dyne/cm.

APPENDIX E
ANALYSIS OF THE BUBBLE ABSORBER

The bubble absorber was analyzed by solving the diffusion, mass, concentration and energy balance equations simultaneously. The complexity of the bubble dynamics lead to difficulties while modeling the absorber. However the model has been simulated using MatLAB and the simulations were run for two different inlet bulk liquid temperatures viz., 114^{o}F (318.56 ^{o}K) and 80 ^{o}F (300 ^{o}K).

The results showed that there is a considerable decrease in the height (the decrease in height was found to be ~20%) of the absorber by sub-cooling the bulk liquid temperature. However in both the cases a jump has been noticed in the ratio of ammonia molar flux absorbed to the total molar flux absorbed/desorbed at around 0.2m from the bottom (Figures. E.3 and E.10). The same jump has been noticed in the graphs corresponding to the mass fraction. The behavior of the bubble diameter is not as expected. Hence there might be a possibility that the assumed correlation is not applicable in this case. More details are to be explored in the area of bubble dynamics. From the figures E.7 and E.14, it can be seen that the vapor temperature is the highest while the coolant temperature is more or less constant. The mass flow rate of the coolant is varied and hence that might be a reason for constant coolant temperature. However this needs to be verified by more simulations and experimental analysis.

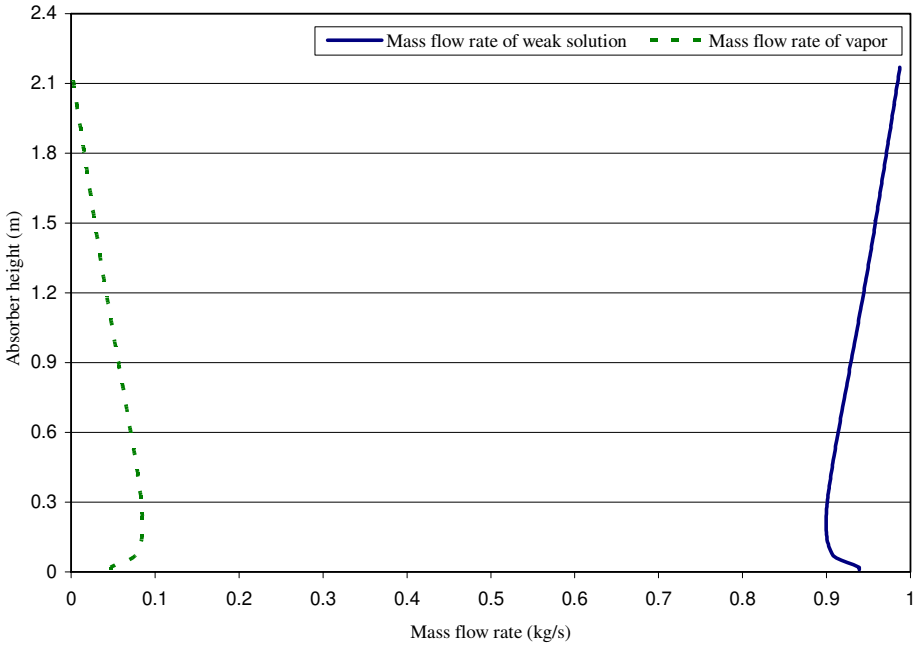

Figure E.1. Variation of the mass flow rate of ammonia along the absorber height (bulk liquid temperature 114^{o}F)

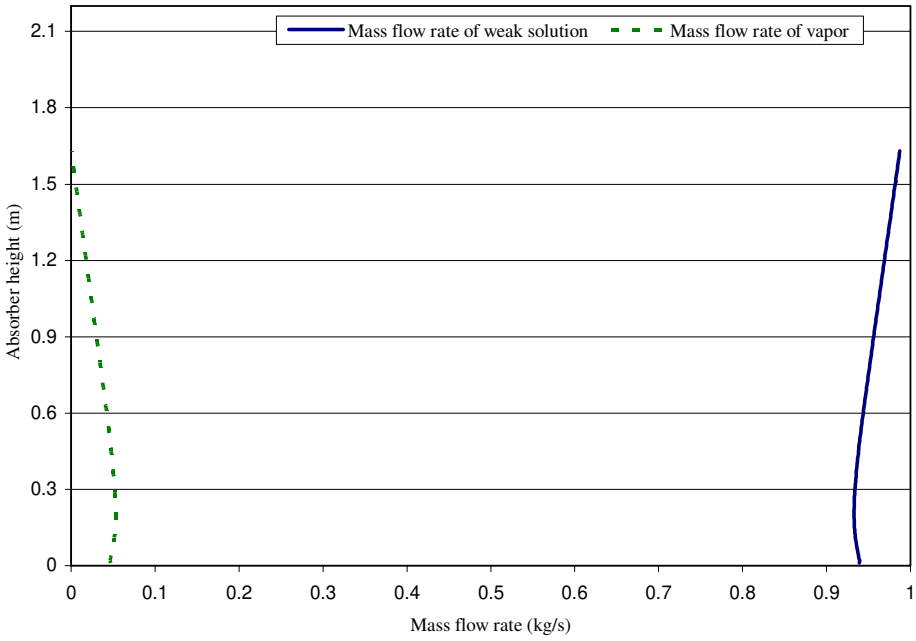

Figure E.2. Variation of the mass flow rate of ammonia along the absorber height (bulk liquid temperature 80^{o}F)

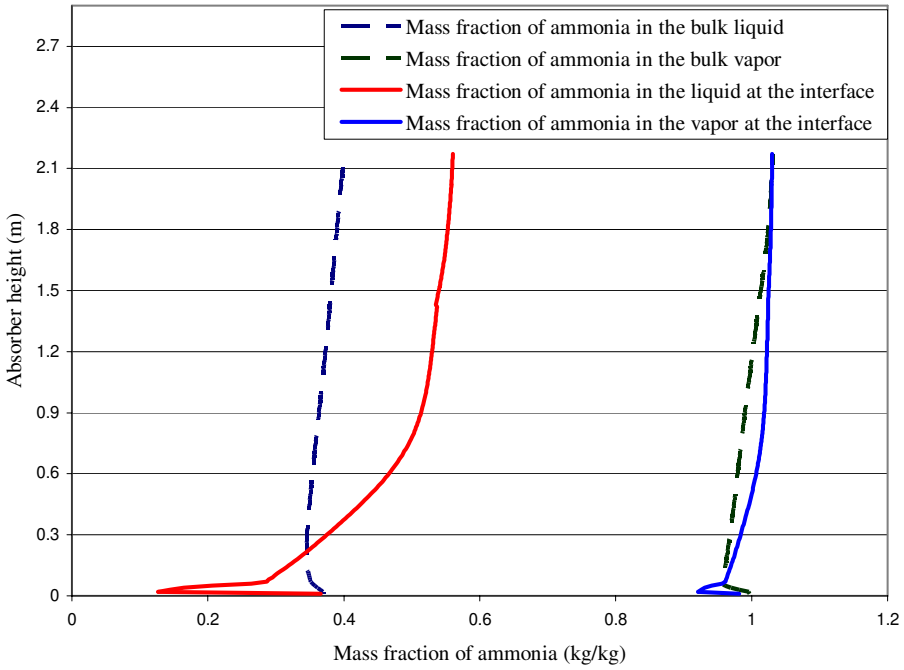

Figure E.3. Variation of mass fraction along the absorber height (bulk liquid temperature 114°F)

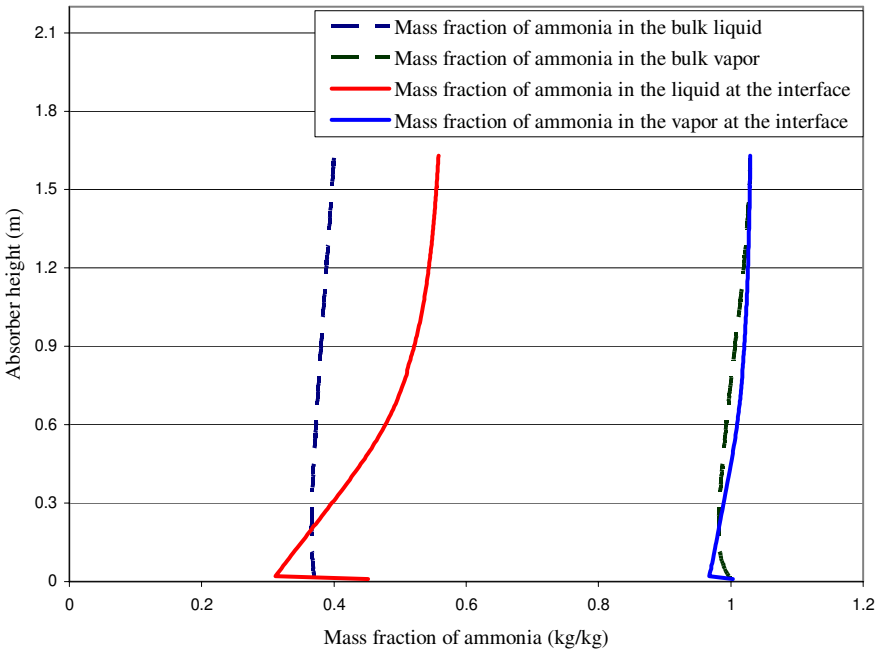

Figure E.4. Variation of mass fraction along the absorber height (bulk liquid temperature 80°F)

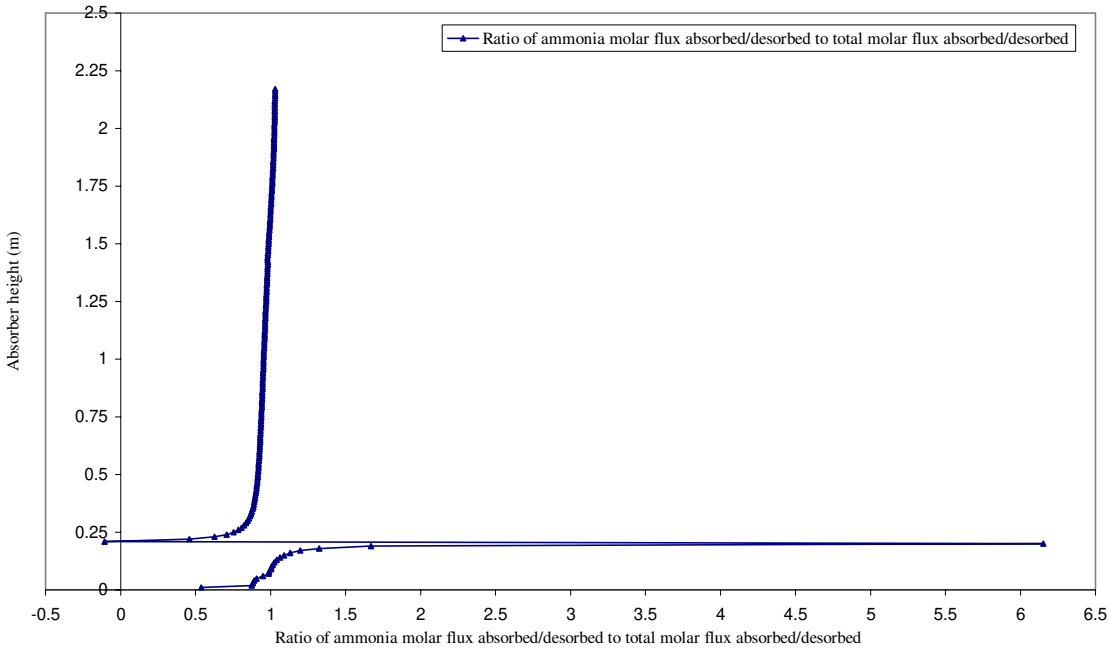

Figure E.5. Variation of the ratio of ammonia molar flux absorbed/desorbed to the total molar flux absorbed/desorbed (bulk liquid temperature 114°F))

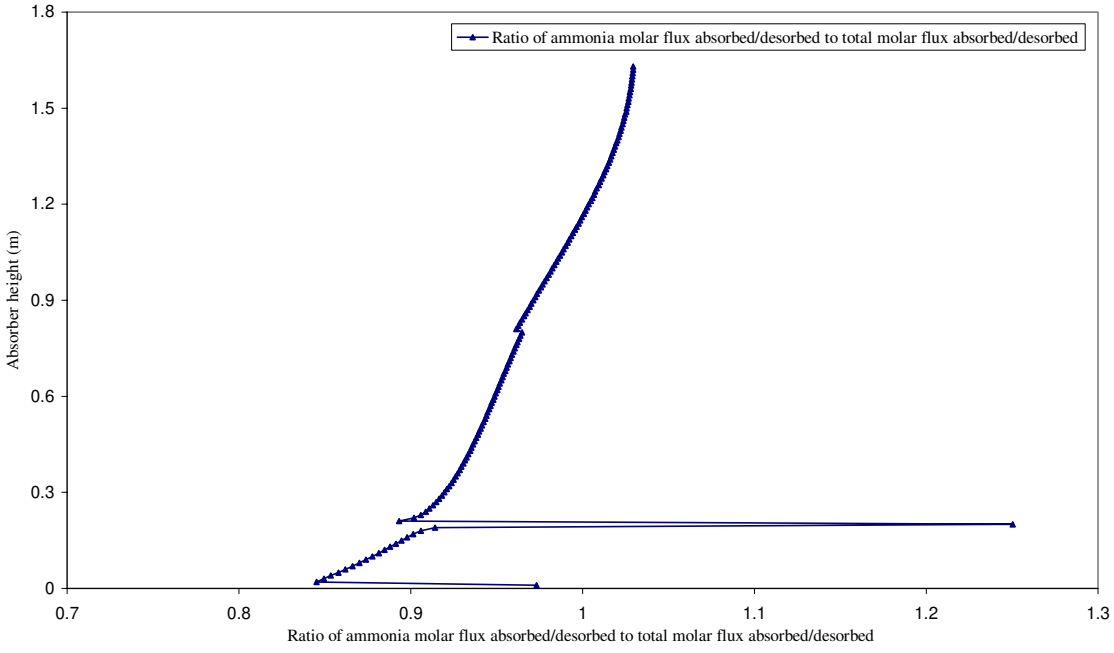

Figure E.6. Variation of the ratio of ammonia molar flux absorbed/desorbed to the total molar flux absorbed/desorbed (bulk liquid temperature 80°F)

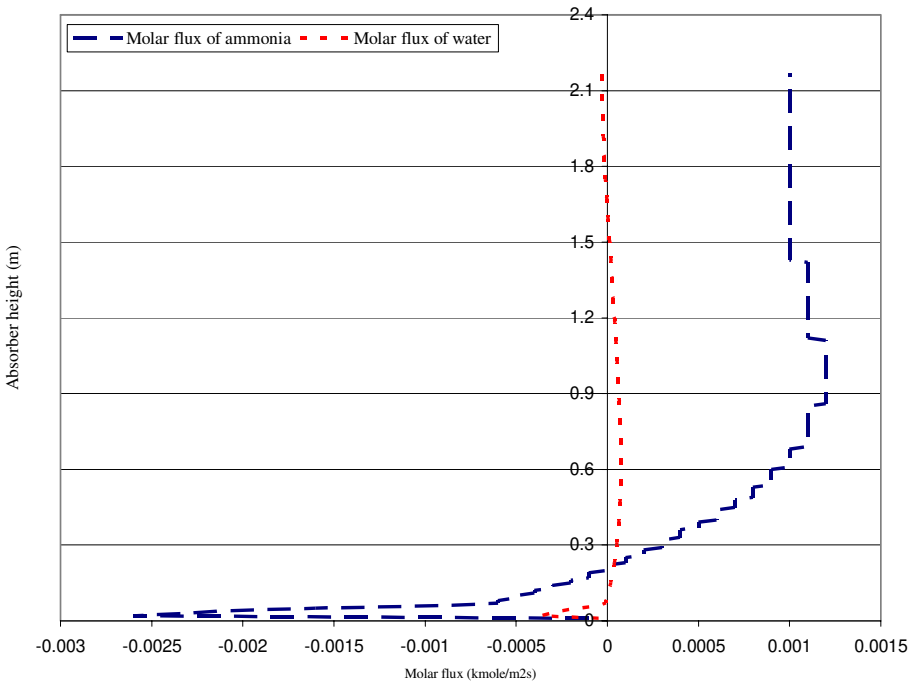

Figure E.7. Variation of molar flux of ammonia and water along the absorber height (bulk liquid temperature 114^{o}F)

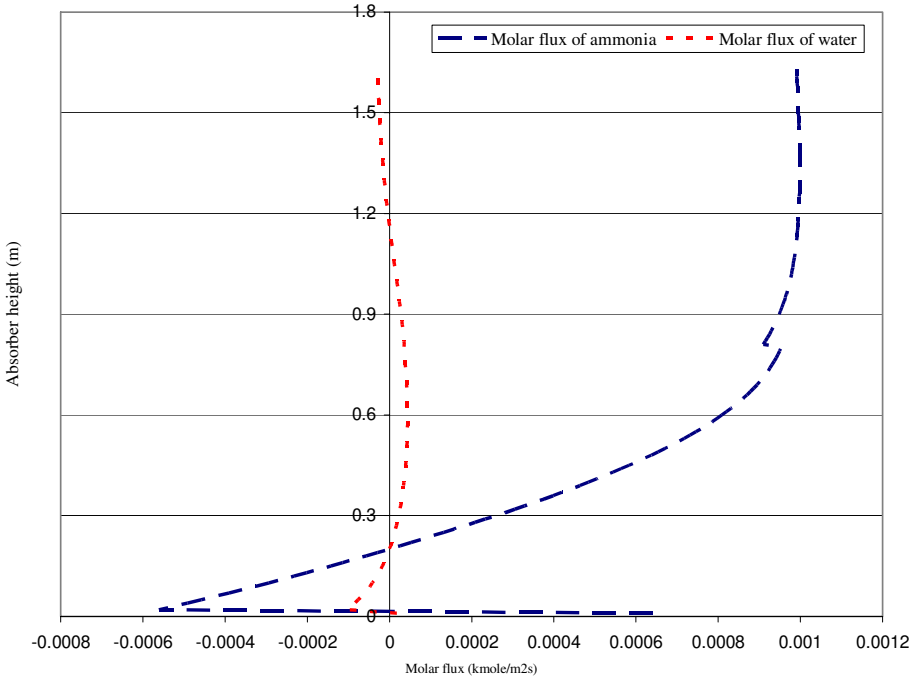

Figure E.8. Variation of molar flux of ammonia and water along the absorber height (bulk liquid temperature 80^{o}F)

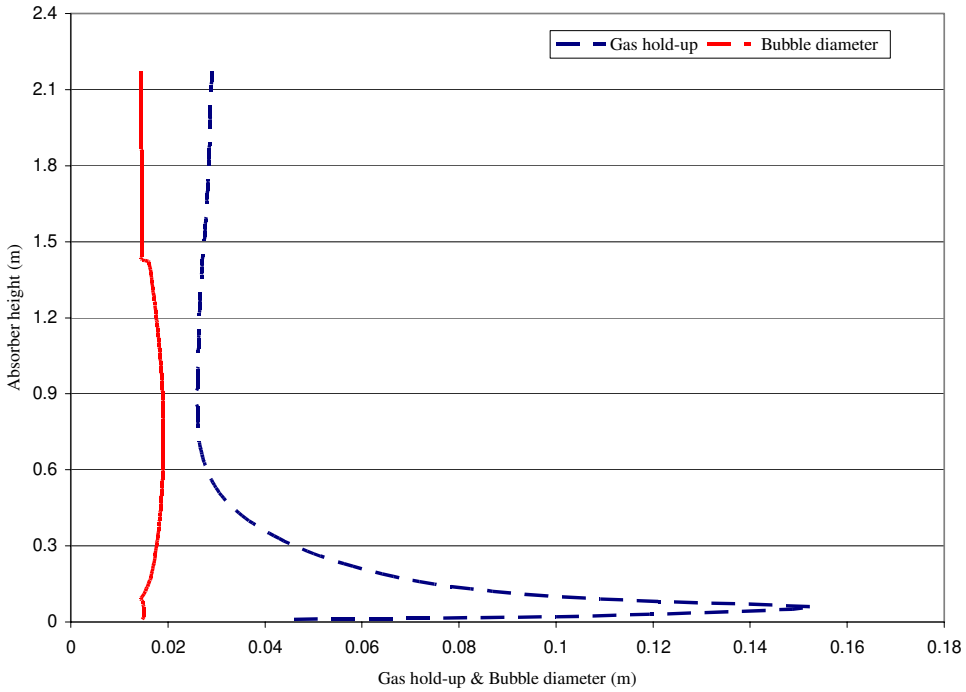

Figure E.9. Variation of gas hold-up and bubble diameter along absorber height (bulk liquid temperature 114°F)

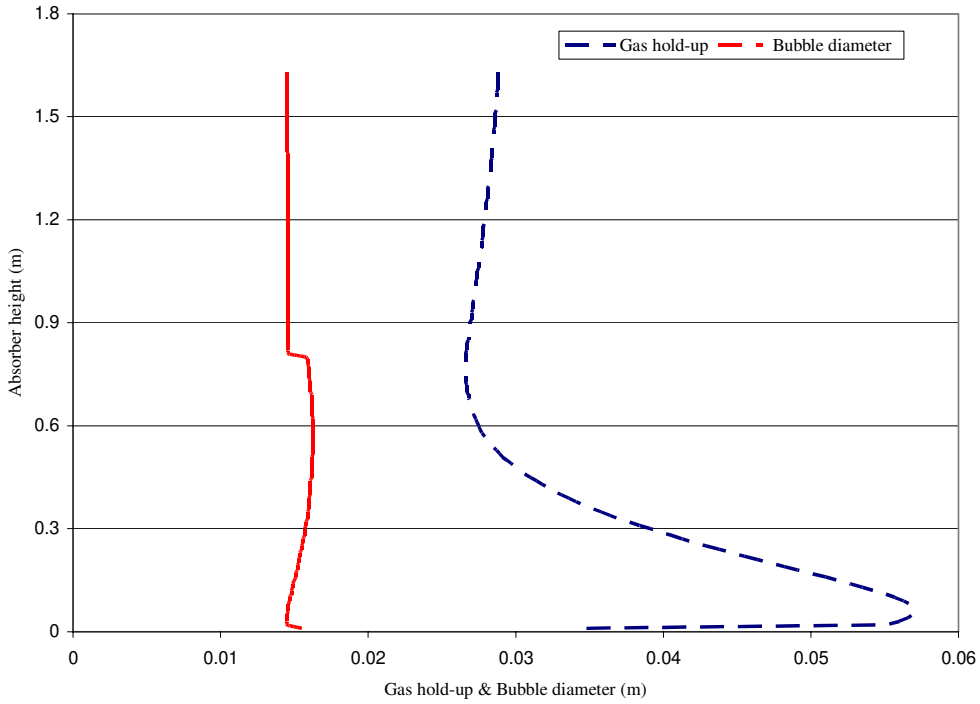

Figure E.10. Variation of gas hold-up and bubble diameter along absorber height (bulk liquid temperature 80°F)

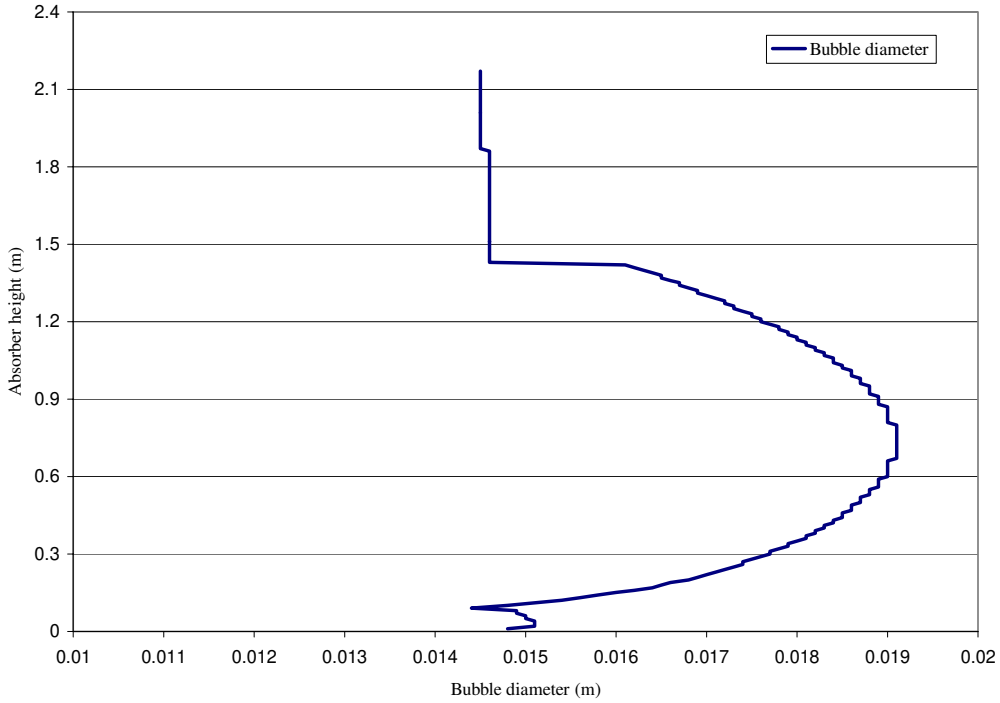

Figure E.11. Variation of bubble diameter along the absorber height (bulk liquid temperature 114^{o}F)

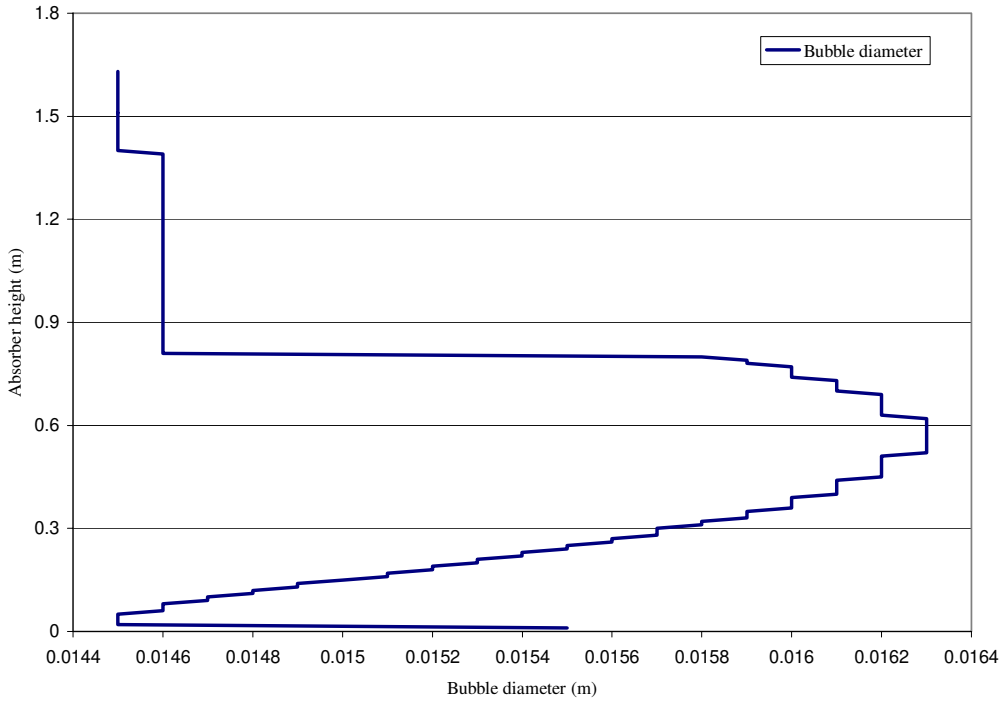

Figure E.12. Variation of bubble diameter along the absorber height (bulk liquid temperature 80oF)

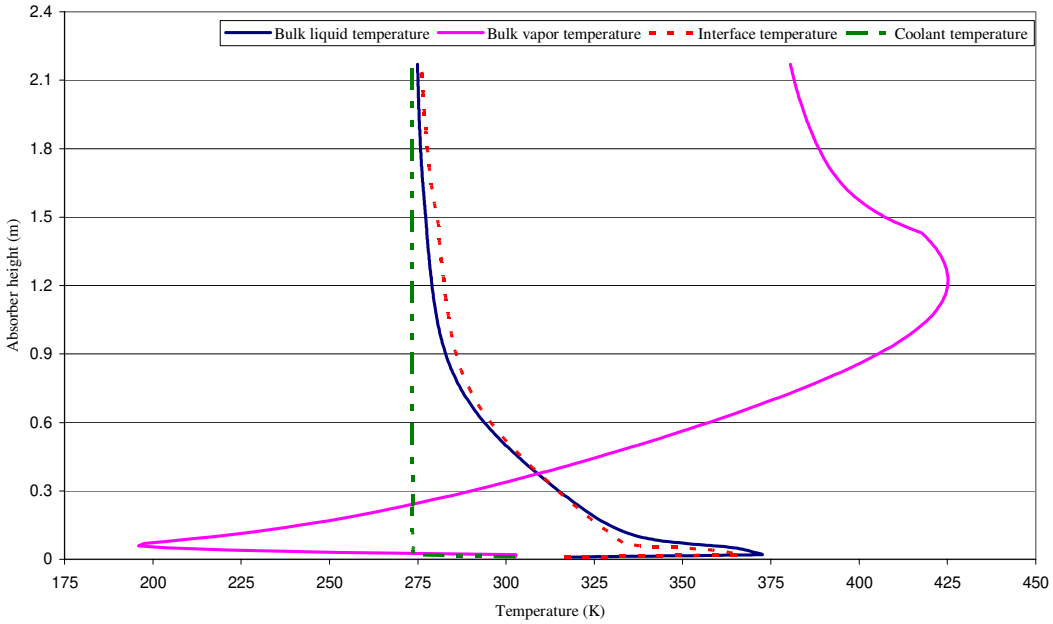

Figure E.13. Temperature variation along the absorber length (bulk liquid temperature 114°F)

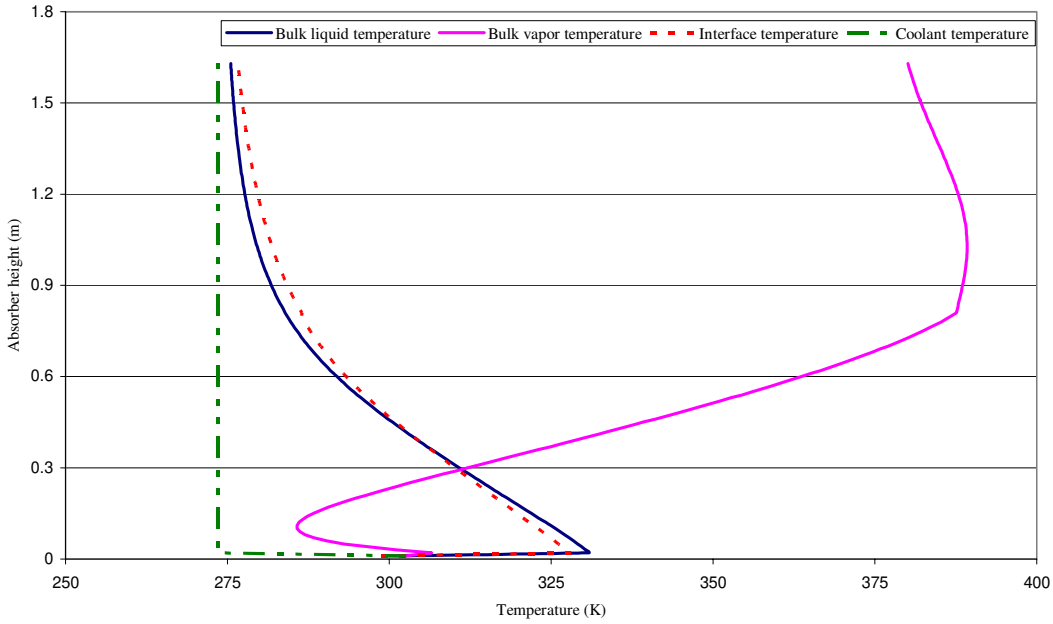

Figure E.14. Temperature variation along the absorber length (bulk liquid temperature 80°F)

```
fprintf('*       Design parameters of a bubble absorber           *\n');
fprintf('*        Code written by Sirisha Govindaraju             *\n');
fprintf('*  Transport property code written in C++ by Goel Nitin   *\n');
fprintf('Thermodynamic property code written in C++ by Gunner Tamm *\n');
fprintf('*        Adapted to MatLAB by Robert Reed                *\n');
fprintf('* Transport and Thermodynamic property code adapted to the current program by
Sirisha Govindaraju               *\n');
fprintf('*               April 18, 2005                           *\n');


format long e;
clear all;
close all;
clc;

%   Reference value for reduced properties
    Tb = 100; %(K)
    Pb = 10; %(bar)
    P = 2.76; %(bar), pressure in the absorber
    R = 8.314; %(KJ/kmol K), universal gas constant
    g = 9.81; %(m/s^2), acceleration due to gravity

%   Gibbs Coefficients for ammonia
    Aa = [3.971423e-2, -1.790557e-5, -1.308905e-2, 3.752836e-3];
    Ba = [1.634519e+1, -6.508119, 1.448937];
    Ca = [-1.049377e-2, -8.288224, -6.647257e+2, -3.045352e+3];
    Da = [3.673647, 9.989629e-2, 3.617622e-2];
    h_rol_a = 4.878573;
    h_rog_a = 26.468873;
    T_ro_a = 3.2252;
    P_ro_a = 2.000;

%   Gibbs Coefficients for water
    Aw = [2.748796e-2, -1.016665e-5, -4.452025e-3, 8.389246e-4];
    Bw = [1.214557e+1, -1.898065, 2.911966e-1];
    Cw = [2.136131e-2, -3.169291e+1, -4.634611e+4, -0.0];
    Dw = [4.019170, -5.175550e-2, 1.951939e-2];
    h_rol_w = 21.821141;
    h_rog_w = 60.965058;
    T_ro_w = 5.0705;
    P_ro_w = 3.000;
    E = [-4.626129e+1, 2.060225e-2, 7.292369, -1.032613e-2, 8.074824e+1, -8.461214e+1,
2.452882e+1, 9.598767e-3, -1.475383, -5.038107e-3, -9.640398e+1, 1.226973e+2, -7.582637,
6.012445e-4, 5.487018e+1, -7.667596e+1];


    mwa = 17.031; %(kg/kmole), molecular weight of ammonia
    mww = 18.015; %(kg/kmole), molecular weight of water

%   Design of absorber
    % Design parameters
    d_o = 0.075; %(m), diameter of orifice
```

```
    n_o = 900; %number of orifice
    Dcm = 0.164; %(m), hydraulic diameter
    a_o = pi*d_o*d_o/4; %(sq.m), area of orifice

    xfsat(1) = [0.3996]; %(kg/kg), required mass fraction of ammonia in the saturated solution
    mfsat(1) = [0.98591]; %(kg/s), required mass flow of saturated ammonia solution
    xlbulk = [0.3696]; %(kg/kg), mass fraction of ammonia in the weak solution at the inlet
    xvbulk = [0.9999]; %(kg/kg), mass fraction of ammonia in the vapor at the inlet
    mvbulk = [0.046919]; %(kg/s) mass flow rate of vapor at the inlet
    mlbulk = [0.93899]; %(kg/s) mass flow rate of weak solution at the inlet
    h_f(1) = -11.63; %(kJ/kg) required specific enthalpy of saturated solution at the outlet

    tvb(1) = 85; %(F), bulk vapor temperature at the inlet
    tvbulk(1) = ((tvb(1)-32)*5/9)+273.15; %(K)
    tlb(1) = 80; %(F), bulk weak solution temperature at the inlet
    tlbulk(1) = ((tlb(1)-32)*5/9)+273.15; %(K)
    tf = 100; %(F), saturated solution temperature at the outlet
    tfinal = ((tf-32)*5/9)+273.15; %(K)
    tc(1) = 85; %(F), coolant temperature at the inlet
    tc(1) = ((tc(1)-32)*5/9)+273.15; %(K)

    %   Reduced properties
    Trm(1) = tlbulk(1)/Tb;
    Trv(1) = tvbulk(1)/Tb;
    Trc(1) = tc(1)/Tb;
    Pr = P/Pb;

    Y(1) = (xlbulk(1)/mwa)/((xlbulk(1)/mwa)+((1-xlbulk(1))/mww)); %mole fraction of ammonia
    molfrw(1) = 1-Y(1); %mole fraction of water
    molfra(1) = Y(1); %mole fraction of ammonia
    mw(1) = molfrw(1) * mww + molfra(1) * mwa; %molecular weight of the mixture

    %   Enthalpy
    hLw(1) = -R*Tb*1000*(-h_rol_w + Bw(1)*(T_ro_w - Trm(1)) + Bw(2)/2*(T_ro_w^2 - Trm(1)^2) + Bw(3)/3*(T_ro_w^3 - Trm(1)^3) - (Aw(1) + Aw(4)*Trm(1)^2)*(Pr-P_ro_w) - Aw(2)/2*(Pr^2 - P_ro_w^2)); %(J/kmole), enthalpy of water(w) in liquid state
    hLa(1) = -R*Tb*1000*(-h_rol_a + Ba(1)*(T_ro_a - Trm(1)) + Ba(2)/2*(T_ro_a^2 - Trm(1)^2) + Ba(3)/3*(T_ro_a^3 - Trm(1)^3) - (Aa(1) + Aa(4)*Trm(1)^2)*(Pr-P_ro_a) - Aa(2)/2*(Pr^2 - P_ro_a^2)); %(J/kmole), enthalpy of ammonia(a) in liquid state
    hga(1) = (-R*Tb*1000/mwa)*(-h_rog_a + Da(1)*(T_ro_a - Trv(1)) + Da(2)/2*(T_ro_a^2 - Trv(1)^2) + Da(3)/3*(T_ro_a^3 - Trv(1)^3) - Ca(1)*(Pr - P_ro_a) - 4*Ca(2)*(Pr*Trv(1)^-3 - P_ro_a*T_ro_a^-3) - 12*Ca(3)*(Pr*Trv(1)^-11 - P_ro_a*T_ro_a^-11) - 4*Ca(4)*(Pr^3*Trv(1)^-11 - P_ro_a^3*T_ro_a^-11)); %(J/kg), enthalpy of ammonia(a) in gaseous state
    hE(1) = -R*Tb*1000*Y(1)*(1-Y(1))*(-E(1) - E(2)*Pr - 2*E(5)/Trm(1) - 3*E(6)*Trm(1)^-2 + (2*Y(1) - 1)*(-E(7) - E(8)*Pr - 2*E(11)/Trm(1) - 3*E(12)*Trm(1)^-2) + (2*Y(1) - 1)^2*(-E(13) - E(14)*Pr - 2*E(15)/Trm(1) - 3*E(16)*Trm(1)^-2)); % (J/kmole) excess enthalpy
    hLm(1) = Y(1)*hLa(1) + (1-Y(1))*hLw(1) + hE(1); %(J/kmole), enthalpy of mixture in liquid state
```

```
    hLm(1) = hLm(1)/((1-xlbulk(1))*mww+(xlbulk(1))*mwa); %(J/kg)
    hLw(1) = hLw(1)/mww; %(J/kg)
    hLa(1) = hLa(1)/mwa; %(J/kg)
    hLc(1) = -R*Tb*1000*(-h_rol_w + Bw(1)*(T_ro_w - Trc(1)) + Bw(2)/2*(T_ro_w^2 - Trc(1)↙
^2) + Bw(3)/3*(T_ro_w^3 - Trc(1)^3) - (Aw(1) + Aw(4)*Trc(1)^2)*(Pr-P_ro_w) - Aw(2)/2*(Pr^2↙
- P_ro_w^2)); %(J/Kmole), Enthalpy of coolant(c) in liquid state
    hLc(1) = hLc(1)/mww; %(J/kg)

    i=1;

    while  mvbulk(i) > 0
        Y(i) = (xlbulk(i)/mwa)/((xlbulk(i)/mwa)+((1-xlbulk(i))/mww)); %mole fraction of↙
ammonia
        molfrw(i) = 1-Y(i); %mole fraction of water
        molfra(i) = Y(i); %mole fraction of ammonia
        mw(i) = molfrw(i) * mww + molfra(i) * mwa; %molecular weight of the mixture

        %   Density
        vLw(i) = R*Tb*(Aw(1) + Aw(3)*Trm(i) + Aw(4)*Trm(i)^2 + Aw(2)*Pr)/Pb; %(m^3/kmole),↙
molar volume of water in liquid state
        vLw(i) = vLw(i)/100;
        dLw(i) = mww/vLw(i);
        vLa(i) = R*Tb/Pb*(Aa(1) + Aa(3)*Trm(i) + Aa(4)*Trm(i)^2 + Aa(2)*Pr); %(m^3/kmole),↙
molar volume of ammonia in liquid state
        vLa(i) = vLa(i)/100;
        vga(i) = R*Tb/Pb*(Trv(i)/Pr + Ca(1) + Ca(2)*Trv(i)^-3 + Ca(3)*Trv(i)^-11 + Ca(4)↙
*Pr^2*Trv(i)^-11);
        vga(i) = vga(i)/100;


        vE(i) = R*(Tb/Pb)*Y(i)*(1-Y(i))*(E(2) + E(4)*Trm(i) + (2*Y(i) - 1)*(E(8) + E(10)↙
*Trm(i)) + (2*Y(i) - 1)^2*E(14));%(m^3/Kmole), Excess molar volume
        vE(i) = vE(i)/100;
        vLm(i) = Y(i)*vLa(i)+ (1-Y(i))*vLw(i) + vE(i); %(m^3/Kmole), Molar volume of↙
mixture in liquid state
        dga(i) = mwa/vga(i); %(kg/m^3) density of gaseous ammonia
        dLm(i) = ((1-xlbulk(i))*mww+(xlbulk(i))*mwa)/vLm(i); %(kg/m^3) density of liquid↙
mixture
        D(i) = dLm(i)-dga(i); % (kg/m^3)


        %   Specific Heat
        cpwl(i) =  Bw(2)*Trm(i) - Bw(3)*Trm(i)*Trm(i) - Bw(1) - 2*Bw(2)*Trm(i) + 2*Aw(4)↙
*Trm(i)*(Pr - P_ro_w); %(no units) Specific heat of water in liquid state
        cpw_l(i) = -R*cpwl(i); %(KJ/Kmole K)
        cpw_l_kg(i) = cpw_l(i)/mww; %(KJ/kg K)
        cpw_v(i) = Dw(2)*Trv(i) - Dw(3)*Trv(i)*Trv(i) - Dw(1)- 2*Dw(2)*Trv(i) + Cw(2)↙
*12*Pr*Trv(i)^(-4) + Cw(3)*12*11*Pr*Trv(i)^(-12)+ Cw(4)*44*Pr^(3)*Trv(i)^(-12); %(no↙
units) Specific heat of water in vapor state
        cpw_v(i) = -R*cpw_v(i); %(KJ/Kmole K)
        cpw_v_kg(i) = cpw_v(i)/mww; %(KJ/kg K)
```

```
        cpal(i) =  Ba(2)*Trm(i) - Ba(3)*Trm(i)*Trm(i) - Ba(1) - 2*Ba(2)*Trm(i) + 2*Aa(4)*Trm(i)*(Pr - P_ro_a); %(no units) Specific heat of ammonia in liquid state
        cpa_l(i) = -R*cpal(i);%(KJ/Kmole K)
        cpa_l_kg(i)=cpa_l(i)/mwa; %(KJ/kg K)
        cpav(i) =  Da(2)*Trv(i) - Da(3)*Trv(i)*Trv(i) - Da(1)- 2*Da(2)*Trv(i) + Ca(2)*12*Pr*Trv(i)^(-4) + Ca(3)*12*11*Pr*Trv(i)^(-12)+ Ca(4)*44*Pr^(3)*Trv(i)^(-12); %(no units) Specific heat of ammonia in vapor state
        cpa_v(i) = -R*cpav(i); %(KJ/Kmole K)
        cpa_v_kg(i)=cpa_v(i)/mwa; %(KJ/kg K)
        f1(i) = -2*E(5)/(Trm(i)*Trm(i)) - 6*E(6)/(Trm(i)*Trm(i)*Trm(i));
        f2(i) = -2*E(11)/(Trm(i)*Trm(i)) - 6*E(12)/(Trm(i)*Trm(i)*Trm(i));
        f3(i) = -2*E(15)/(Trm(i)*Trm(i)) - 6*E(16)/(Trm(i)*Trm(i)*Trm(i));
        cpe(i) = R*(f1(i) + f2(i)*(2*Y(i) - 1) + f3(i)*(2*Y(i) - 1)*(2*Y(i) - 1))*(1 - Y(i))*Y(i); %(KJ/Kmole K) Excess specific heat
        cpmix_l(i) = cpw_l(i)*molfrw(i) + cpa_l(i)*molfra(i) + cpe(i); %(KJ/Kmole K) Specific heat of liquid mixture
        cpmix_l_kg(i)=  cpmix_l(i)/mw(i);


        %   Thermal conductivity
        kwl(i) = -0.2758 + (4.612e-3)*tlbulk(i) - (5.5391e-6)*tlbulk(i)*tlbulk(i); %(W/mK), thermal conductivity of water in liquid state
        kal(i) = 1.1606 - (2.284e-3)*tlbulk(i) + (3.1245e-18)*tlbulk(i)*tlbulk(i); %(W/mK), thermal conductivity of ammonia in liquid state
        kav(i) = 0.00457 + (2.3239e-5)*tvbulk(i) + (1.481e-7)*tvbulk(i)*tvbulk(i); %(W/mK), thermal conductivity of ammonia in vapor state

        %Correlation is valid only if k1>k2
        alpha = 1; %characteristic parameter of the binary mixture and can be taken as unity if the experimental data is unavailable

            if kwl(i)>kal(i)
                k1(i) = kal(i);
                k2(i) = kwl(i);
                y1(i) = xlbulk(i);
                y2(i) = 1-xlbulk(i);
            else
                k1(i) = kwl(i);
                k2(i) = kal(i);
                y1(i) = 1-xlbulk(i);
                y2(i) = xlbulk(i);
            end
                kmixl(i) = y1(i)*k1(i)+y2(i)*k2(i)-alpha*(k2(i)-k1(i))*(1-(y2(i))^0.5)*(y2(i)); %(W/mK), thermal conductivity of mixture in liquid state

        %   Viscosity
        mu_l(i)= ((0.67+0.78*Y(i))*1e-6)*exp(17900/(R*tlbulk(i))); %(PaS), dynamic viscosity of liquid mixture
        mu_v(i) = (-7.8737+((3.6745*1e-1)*tvbulk(i))-((4.4729*1e-6)*tvbulk(i)*tvbulk(i))); %(Micropoise), dynamic viscosity of gas
        mu_v(i) = mu_v(i)*0.1e-6;  %(Pa S), dynamic viscosity of gas
```

```
        %   Diffusivity
        M12 = ((1/mwa)+(1/mww))^(1/2);
        sv2 = 14.9;
        sv1 = 12.7;
        D_av(i) = 0.00100*(tvbulk(i)^1.75)*(M12)/(Pb*((sv1)^(1/3)+(sv2)^(1/3))^2); %↙
diffusivity is in cm^2/s
        D_av(i) = D_av(i)*1e-4;  % diffusivity is in m^2/s
        D_awl(i)=((1.65+2.47*Y(i))*1e-6)*exp(-16600/R/tlbulk(i)); % (m^2/s) Diffusivity↙
for ammonia/water liquid

        %   Surface Tension
        s_tension_a=44.45e-3; %(N/m), Surface tension of ammonia
        s_tension_w=0.0728; %(N/m), Surface tension of water
        s_tension(i)=(xlbulk(i)*s_tension_a)+((1-xlbulk(i))*s_tension_w)-((s_tension_w-↙
s_tension_a)*((1.442*(1-xlbulk(i))*(1-exp(-2.5*(xlbulk(i))^4)))+(1.106*xlbulk(i)*(1-exp↙
(-2.5*(1-(xlbulk(i)))^6)))))%(N/m), surface tension of the mixture

        %   Calculation of bubble diameter using Bhavaraju's correlation
        qvbulk(i)=mvbulk(i)/(dga(i)); %(m3/s), volumetric flow rate of the gas
        qvbulk_o(i)=qvbulk(i)/n_o; %(m3/s), volumetric flow rate of the gas per orifice


        dia_b(i)=(6*s_tension(i)*d_o/(g*D(i)))^(1/3); %(m), diameter of the bubble
        v_v1(i)=(g*dLm(i)/(18*mu_l(i)))*(dia_b(i)^2); %(m/s), velocity of the bubble
        v_v2(i)=((2*s_tension(i)/(dLm(i)*dia_b(i)))+(g*dia_b(i)/2))^0.5; %(m/s), velocity↙
of the bubble

        Re_v1(i) = (dga(i)*v_v1(i)*dia_b(i))/mu_v(i); %Reynold's number of vapor
        Re_v2(i) = (dga(i)*v_v2(i)*dia_b(i))/mu_v(i); %Reynold's number of vapor

            if Re_v1(i)>1
                v_v(i)=v_v2(i);
                Re_v(i)=Re_v2(i);
            else
                v_v(i)=v_v1(i);
                Re_v(i)=Re_v1(i);
            end

            if Re_v(i) <= 1.0
                qvbulk_t(i)=(pi*g*D(i)*(dia_b(i))^4)/(108*mu_l(i)); %(m^3/s)
            else
                qvbulk_t(i)=0.32*(g^0.5)*(dia_b(i))^(5/2);
            end

            Re_l(i) = 4*dLm(i)*qvbulk_o(i)/(pi*d_o*mu_l(i)); %liquid reynold's number
            Fr(i) = qvbulk_o(i)^2/(d_o^5*g); %Froude's number
            d_vs(i)=26*Dcm*(Dcm*Dcm*dLm(i)*g/s_tension(i))^(-0.5)*(Dcm^3*dLm(i)^2*g/mu_l↙
(i)^2)^(-0.12)*(v_v(i)/(Dcm*g))^(-0.12); %(m), mean bubble diameter
            dia_b2(i)=d_o*3.23*Re_l(i)^(-0.1)*Fr(i)^0.21;
```

```
            if qvbulk_o(i)<qvbulk_t(i)
                d_b(i) = dia_b(i); %(m),diameter of the bubble
            else if (qvbulk_o(i)>qvbulk_t(i)) & (Re_l(i)<2000)
                d_b(i) = dia_b2(i);
                else if (qvbulk_o(i)>qvbulk_t(i)) & (Re_l(i)>2000)
                    if d_b(i-1)<d_vs(i)
                        d_b(i)=d_o*3.23*Re_l(i)^(-0.1)*Fr(i)^0.21
                        else if (d_vs(i)<d_b(i-1)) & (d_vs>0.0045 )
                            d_b(i)=d_vs(i)
                            else if d_vs(i)<0.0045
                                d_b(i)=0.0045
                            end
                        end
                    end
                end
            end


        %   Calculation of the gas hold-up
        v_bs(i) = (s_tension(i)*2.25/mu_l(i))*(s_tension(i)^(3)*(dLm(i))/(g*mu_l(i)^(4)))^↙
(-0.273)*(dLm(i)/dga(i))^0.03; %(m/s), velocity of small bubble
        v_trans(i) = 0.5*v_bs(i)*exp(-193*(dga(i)^(-0.61))*(mu_l(i)^(0.5))*(s_tension(i)^↙
(0.11))); %(m/s), transition velocity
        v_bl(i) = (s_tension(i)*(((v_bs(i)*mu_l(i))/s_tension(i))+(2.4*((mu_l(i)*(v_v(i)-↙
v_trans(i)))/(s_tension(i)))^(0.757))+(((s_tension(i)^(3))*dLm(i))/(g*(mu_l(i))^(4)))^↙
(-0.077)*(dLm(i)/dga(i))^(0.077)))/(mu_l(i)); %(m/s), velocity of large bubble
            if v_v(i)<=v_trans(i)
                gas_holdup(i) = v_v(i)/v_bs(i);
            else
                gas_holdup(i) = ((v_trans(i)/v_bs(i))+((v_v(i)-v_trans(i))/v_bl(i)));
            end

        %   Calculation of liquid-vapor interfacial area
        delta_l = 0.01; %(m) length of the differential element
        a_c = 0.09*0.9106; % cross sectional area of the absorber
        abs_ht(i) = i*0.01; %(m) absorber height
        a_i(i)=6*gas_holdup(i)/d_vs(i); %(m2/m3) interfacial area
        delta_a_m(i) = a_i(i)*a_c*delta_l;

        St_l(i) = 0.01*(dLm(i)*v_v(i)*d_b(i)/mu_l(i))^(-0.25)*(v_v(i)*v_v(i)/g/d_b(i))^↙
(-0.25)*(mu_l(i)*cpmix_l(i)/kmixl(i))^(-0.5); % stanton number in the bulk liquid
        Pr_v(i) = mu_v(i)*cpa_v_kg(i)*1000/kav(i); % prandtl number in the vapor
        Pr_l(i) = mu_l(i)*cpmix_l_kg(i)*1000/kmixl(i); % prandtl number in the liquid
        Sc_v(i) = mu_v(i)/dga(i)/D_av(i); % schimdt's number in the vapor
        Sc_l(i) = mu_l(i)/dLm(i)/D_awl(i); % Schimdt's number in the bulk liquid

        a_s(i) = 4*pi*(d_b(i)/2)^2; %(sq.m), surface area of bubble
        a_p(i) = pi*(d_b(i)/2)^2; %(sq.m), projected area of the bubble

        c_m_mix(i) = dLm(i)/mw(i); %(kg mole/m^3), Molar density = density/molecular↙
```

```
weight
        c_m_a(i) = dga(i)/mwa; %(kg mole/m^3), Molar density = density/molecular weight

        %   Calculation of heat transfer coefficient of ammonia vapor mixture
        h_v(i) = (1.4*1000*c_m_a(i)*a_s(i)*cpa_v(i)*(Sc_v(i)/Pr_v(i))^(2/3)*(48*s_tension↙
(i)*(D_av(i))^2/(pi*pi*(d_b(i)^3)*dLm(i)*(2+3*(dga(i)/dLm(i)))))^(0.25))/(a_p(i));  %↙
(W/m^2 K), heat transfer coefficient of the vapor

        %   Calculation of volumetric mass transfer coefficient of the liquid phase
        F_l_ms(i) = (0.5*D_awl(i)*(mu_l(i)/(dLm(i)*D_awl(i)))^0.5*((g*(d_b(i)^3)*(dLm(i)↙
*dLm(i)))/(mu_l(i)*mu_l(i)))^(0.25)*(g*d_b(i)*d_b(i)*dLm(i)/s_tension(i))^(3/8))/(6*d_b↙
(i)); %(m/s), volumetric mass transfer coefficient in liquid state
        F_l(i)=F_l_ms(i)*c_m_mix(i); %(Kmole/m^2 s)

        %   Calculation of heat transfer coefficient of liquid mixture
        h_l(i)=cpmix_l(i)*1000*F_l(i)*(Sc_l(i)/Pr_l(i))^(2/3);  %(W/m^2 K), heat transfer↙
coefficient of the liquid

        %   Volumetric mass transfer coefficient from Clift et. al. correlation (m/s)
        F_v_ms(i) = ((48*s_tension(i)*(D_av(i))^2/(pi*pi*(d_b(i)^3)*dLm(i)*(2+3*(dga(i)↙
/dLm(i)))))^(0.25))*1.4*a_s(i)/(a_p(i)) ; %(m/s), volumetric mass transfer coefficient of↙
vapor
        F_v(i)=F_v_ms(i)*c_m_a(i); %(Kmole/m^2 s)

        ti(i)=[115]; %(deg F), guessed interface temperature
        xli(i)=(0.38-2.667e-3*(ti(i)-105)); %(kg/kg), mass fraction of ammonia in the↙
liquid at the interface
        xvi(i)=(0.985-6.67e-4*(ti(i)-105)); %(kg/kg), mass fraction of ammonia in the↙
vapor at the interface


        %   Diffusion and Concentration balance equation
        syms t;
        eqn=F_l(i)* log((t-xlbulk(i))/(t-xli(i)))- F_v(i) * log((t-xvi(i))/(t-xvbulk(i)));
        T=solve(eqn,t);
        p(i)=T;
        z(i)=double(p(i));

        N_h3n(i)= z(i)*F_l(i)*log((z(i)-xlbulk(i))/(z(i)-xli(i))); %(kmole/m^2s), Molar↙
flux of ammonia
        N_h2o(i)= (N_h3n(i)/z(i)) - N_h3n(i); %kmole/m2s, Molar flux of water
        k(i)=(F_l(i))*log((z(i)-xlbulk(i))/(z(i)-xli(i)))*delta_a_m(i)  %(kmole/s)

        c_ovb(i) = ((N_h3n(i)*cpa_v(i)+N_h2o(i)*cpw_v(i))*1000)/h_v(i);
        c_olb(i) = ((N_h3n(i)*cpa_l(i)+N_h2o(i)*cpw_l(i))*1000)/h_l(i);
        covb(i) = (c_ovb(i)/(1-exp(-c_ovb(i))))*h_v(i)*delta_a_m(i);
        colb(i) = (c_olb(i)/(1-exp(-c_olb(i))))*h_l(i)*delta_a_m(i);

        %   Enthalpy at the interface
        ti(i) = ((ti(i)-32)*5/9)+273.15; %(deg. K)
        Tri(i)=ti(i)/Tb;
        hLwi(i) = -R*Tb*(-h_rol_w + Bw(1)*(T_ro_w - Tri(i)) + Bw(2)/2*(T_ro_w^2 - Tri(i)↙
```

```
^2) + Bw(3)/3*(T_ro_w^3 - Tri(i)^3) - (Aw(1) + Aw(4)*Tri(i)^2)*(Pr-P_ro_w) - Aw(2)/2*(Pr^2 ↙
- P_ro_w^2)); %( KJ/Kmole), Enthalpy of water(w) in liquid state
        hLai(i) = -R*Tb*(-h_rol_a + Ba(1)*(T_ro_a - Tri(i)) + Ba(2)/2*(T_ro_a^2 - Tri(i) ↙
^2) + Ba(3)/3*(T_ro_a^3 - Tri(i)^3) - (Aa(1) + Aa(4)*Tri(i)^2)*(Pr-P_ro_a) - Aa(2)/2*(Pr^2 ↙
- P_ro_a^2)); %( KJ/Kmole), Enthalpy of ammonia(a) in liquid state
        hgai(i) = -R*Tb*(-h_rog_a + Da(1)*(T_ro_a - Tri(i)) + Da(2)/2*(T_ro_a^2 - Tri(i) ↙
^2) + Da(3)/3*(T_ro_a^3 - Tri(i)^3) - Ca(1)*(Pr - P_ro_a) - 4*Ca(2)*(Pr*Tri(i)^-3 - ↙
P_ro_a*T_ro_a^-3) - 12*Ca(3)*(Pr*Tri(i)^-11 - P_ro_a*T_ro_a^-11) - 4*Ca(4)*(Pr^3*Tri(i)^- ↙
11 - P_ro_a^3*T_ro_a^-11)); %( KJ/Kmole), Enthalpy of ammonia(a) in gaseous state at the ↙
interface
        hgwi(i) = -R*Tb*(-h_rog_w + Dw(1)*(T_ro_w - Tri(i)) + Dw(2)/2*(T_ro_w^2 - Tri(i) ↙
^2) + Dw(3)/3*(T_ro_w^3 - Tri(i)^3) - Cw(1)*(Pr - P_ro_w) - 4*Cw(2)*(Pr*Tri(i)^-3 - ↙
P_ro_w*T_ro_w^-3) - 12*Cw(3)*(Pr*Tri(i)^-11 - P_ro_w*T_ro_w^-11) - 4*Cw(4)*(Pr^3*Tri(i)^- ↙
11 - P_ro_w^3*T_ro_w^-11)); %( KJ/Kmole), Enthalpy of water(w) in gaseous state at the ↙
interface
        hLwi(i) = hLwi(i)/mww; %( kJ/kg)
        hgwi(i) = hgwi(i)/mww; %( kJ/kg)
        hgai(i) = hgai(i)/mwa; %( kJ/kg)
        hLai(i) = hLai(i)/mwa; %( kJ/kg)

        tinew(i)=(-N_h3n(i)*mwa*delta_a_m(i)*hLai(i)*1000-N_h2o(i)*mww*delta_a_m(i)*hLwi ↙
(i)*1000+N_h3n(i)*mwa*delta_a_m(i)*hgai(i)*1000+N_h2o(i)*mww*delta_a_m(i)*hgwi(i) ↙
*1000+tlbulk(i)*colb(i)+tvbulk(i)*covb(i))/(covb(i)+colb(i)); %(K), interface temperature
        tinew(i)=((tinew(i)-273.15)*9/5)+32;  %(deg. F)
        ti(i)=((ti(i)-273.15)*9/5)+32;  %(deg. F)
        while abs(ti(i)-tinew(i)) > 0.00001
            tinew(i)=(-N_h3n(i)*mwa*delta_a_m(i)*hLai(i)*1000-N_h2o(i)*mww*delta_a_m(i) ↙
*hLwi(i)*1000+N_h3n(i)*mwa*delta_a_m(i)*hgai(i)*1000+N_h2o(i)*mww*delta_a_m(i)*hgwi(i) ↙
*1000+tlbulk(i)*colb(i)+tvbulk(i)*covb(i))/(covb(i)+colb(i));
            tinew(i)=((tinew(i)-273.15)*9/5)+32; %(deg. F)
            ti(i)=(tinew(i)+ti(i))/2;
            xli(i)=(0.38-2.667e-3*(ti(i)-105));
            xvi(i)=(0.985-6.67e-4*(ti(i)-105));
        end


        % Recalculating the molar fluxes with the new interface temperature
        eqn=F_l(i)* log((t-xlbulk(i))/(t-xli(i)))- F_v(i) * log((t-xvi(i))/(t-xvbulk(i)));
        T=solve(eqn,t);
        p(i)=T;
        z(i)=double(p(i));
        N_h3n(i)= z(i)*F_l(i)*log((z(i)-xlbulk(i))/(z(i)-xli(i)));
        N_h2o(i)= (N_h3n(i)/z(i)) - N_h3n(i);
        k(i)=(F_l(i))*log((z(i)-xlbulk(i))/(z(i)-xli(i)))*delta_a_m(i);

        % Mass flow for the co-current bubble absorber
        mvbulk(i+1)=mvbulk(i)-(k(i)*dga/c_m_a); %(kg/s) mass flow rate of the bulk vapor
        xvbulk(i+1)=(mvbulk(i)*xvbulk(i)-(k(i)*dga*z(i)/c_m_a))/(mvbulk(i+1)); %(kg/kg) ↙
mass fraction of ammonia in the bulk vapor
        mlbulk(i+1)=mlbulk(i)+(k(i)*dLm(i)/c_m_mix(i)); %(kg/s) mass flow rate of the bulk ↙
liquid
        xlbulk(i+1)=(mlbulk(i)*xlbulk(i)+(k(i)*dLm(i)*z(i)/c_m_mix(i)))/(mlbulk(i+1)); % ↙
```

```
(kg/kg) mass fraction of ammonia in the bulk liquid

        c_ovb(i) = ((N_h3n(i)*cpa_v(i)+N_h2o(i)*cpw_v(i))*1000)/h_v(i);
        c_olb(i) = ((N_h3n(i)*cpa_l(i)+N_h2o(i)*cpw_l(i))*1000)/h_l(i);
        covb(i)=(c_ovb(i)/(1-exp(-c_ovb(i))))*h_v(i)*delta_a_m(i);
        colb(i)=(c_olb(i)/(1-exp(-c_olb(i))))*h_l(i)*delta_a_m(i);
        tiK(i) = ((ti(i)-32)*5/9)+273.15; %(deg. K)
        qsenv(i)=covb(i)*(tvbulk(i)-tiK(i));
        qsenL(i)=colb(i)*(tiK(i)-tlbulk(i));

        % Calculating the enthalpy of vapor
        hga(i+1) = (mvbulk(i)*hga(i)-qsenv(i)-N_h3n(i)*mwa*delta_a_m(i)*hLai(i)*1000-N_h2o↙
(i)*mww*delta_a_m(i)*hLwi(i)*1000)/mvbulk(i+1);
        syms Trvn f;
        f=hga(i+1)-((-R*Tb*1000/mwa)*(-h_rog_a + Da(1)*(T_ro_a - Trvn) + Da(2)/2*(T_ro_a^2↙
- Trvn^2) + Da(3)/3*(T_ro_a^3 - Trvn^3) - Ca(1)*(Pr - P_ro_a) - 4*Ca(2)*(Pr*Trvn^-3 -↙
P_ro_a*T_ro_a^-3) - 12*Ca(3)*(Pr*Trvn^-11 - P_ro_a*T_ro_a^-11) - 4*Ca(4)*(Pr^3*Trvn^-11 -↙
P_ro_a^3*T_ro_a^-11)));
        Trvn=solve(f,Trvn);
        TRV=double(Trvn);
        for j=1:length(TRV)
            if (imag(TRV(j))==0) & (real(TRV(j))>0)
                break
            end
        end
        Trv(i+1) = TRV(j);
        tvbulk(i+1)=Trv(i+1)*Tb;

        Q_in(1) = mvbulk(1)*hga(1)+mlbulk(1)*hLm(1);
        Q_out(1) = mfsat(1)*h_f(1)*1000;
        Q_gen(1) = (Q_in(1)-Q_out(1)); %(J/s) Heat generated due to absorption
        Q_gen_btuh(1) = Q_gen(1)*3.412; %(Btuh) Heat generated due to absorption
        Q_gen_ton(1) = Q_gen_btuh(1)/12000; %(Tons) Heat generated due to absorption

        %   Cooling water requirement
        temp_diff(i) = tlbulk(i)-tc(i); %(deg F) temperature difference between the bulk↙
liquid and the coolant
        gpm(i)=abs(Q_gen_btuh(1)/(500*temp_diff(i))); %(gpm) flow rate of cooling water

        vLc(i) = R*Tb*(Aw(1) + Aw(3)*Trc(i) + Aw(4)*Trc(i)^2 + Aw(2)*Pr)/Pb; %(m^3/Kmole),↙
molar volume of coolant(water) in liquid state
        vLc(i) = vLc(i)/100;
        dLc(i) = mww/vLc(i);
        cpcl(i) =  Bw(2)*Trc(i) - Bw(3)*Trc(i)*Trc(i) - Bw(1) - 2*Bw(2)*Trc(i) + 2*Aw(4)↙
*Trc(i)*(Pr - P_ro_w); %(no units) specific heat of coolant(water) in liquid state
        cpc_l(i) = -R*cpcl(i); %(KJ/Kmole K)
        cpc_l_kg(i) = cpc_l(i)/mww; %(KJ/kg K)

        mc(i)=gpm(i)*6.309020e-5*dLc(i); %(kg/s) mass flow rate of coolant
        vc(i)=mc(i)/(dLc(i)*0.9109*0.010); %(m/s) velocity of coolant

        kcl(i) = -0.2758 + (4.612e-3)*tc(i) - (5.5391e-6)*tc(i)*tc(i); %(W/mK), thermal↙
```

```
conductivity of coolant(water) in liquid state
        mu_c(i)=0.001*10^(-10.2158+(1.79925*1e+3/tc(i))+(1.773*1e-2)*tc(i)-(1.2631*1e-5)↙
*tc(i)^2); %(PaS), dynamic viscosity of coolant(water)

        L=2*0.01*0.9109/(0.9109+0.1);
        Re_p(i)=dLc(i)*vc(i)*L/mu_c(i); %reynold's number of plate
        Pr_c(i) = mu_c(i)*cpc_l_kg(i)*1000/kcl(i); % prandtl number of coolant

        h_c(i)=0.026*(kcl(i)/0.002)*Re_p(i)^0.82*(Pr_c(i)^0.32); %(W/m2K) heat transfer↙
coefficient of coolant

        Ref(i)=4*mc(i)/mu_c(i)/0.01; %film reynold's number

        del(i)=0.8434*Ref(i)^(1/3)*((mu_c(i)/dLc(i))^2/g)^(1/3);
        hfilm(i)=0.029*(kcl(i)/del(i))*Ref(i)^0.533*Pr_c(i)^0.344; %(W/m2K) heat transfer↙
coefficient of film

        res=0.1/15; %(W/m2K) resistance of wall

        U(i)=1/(1/h_c(i)+res+1/hfilm(i)); %(W/m2K) over-all heat transfer coefficient

        Qc(i)= U(i)*0.9109*delta_l*i*(tlbulk(i)-tc(i)); %(W) heat transferred to coolant
        Qc(1)=0;

        % Calculating the enthalpy of liquid mixture
        hLm(i+1) = (mlbulk(i)*hLm(i)+qsenL(i)+N_h3n(i)*mwa*delta_a_m(i)*hLai(i)*1000+N_h2o↙
(i)*mww*delta_a_m(i)*hLwi(i)*1000-Qc(i))/mlbulk(i+1);
        syms Trmn F;
        F=hLm(i+1)-((Y(i)*(-R*Tb*1000*(-h_rol_a + Ba(1)*(T_ro_a - Trmn) + Ba(2)/2*↙
(T_ro_a^2 - Trmn^2) + Ba(3)/3*(T_ro_a^3 - Trmn^3) - (Aa(1) + Aa(4)*Trmn^2)*(Pr-P_ro_a) -↙
Aa(2)/2*(Pr^2 - P_ro_a^2))) + (1-Y(i))*(-R*Tb*1000/mww*(-h_rol_w + Bw(1)*(T_ro_w - Trmn) +↙
Bw(2)/2*(T_ro_w^2 - Trmn^2) + Bw(3)/3*(T_ro_w^3 - Trmn^3) - (Aw(1) + Aw(4)*Trmn^2)*(Pr-↙
P_ro_w) - Aw(2)/2*(Pr^2 - P_ro_w^2))) + (-R*Tb*1000*Y(i)*(1-Y(i))*(-E(1) - E(2)*Pr - 2*E↙
(5)/Trmn - 3*E(6)*Trmn^-2 + (2*Y(i) - 1)*(-E(7) - E(8)*Pr - 2*E(11)/Trmn - 3*E(12)*Trmn^-↙
2) + (2*Y(i) - 1)^2*(-E(13) - E(14)*Pr - 2*E(15)/Trmn - 3*E(16)*Trmn^-2))))/((1-xlbulk(i))↙
*mww+(xlbulk(i))*mwa));
        simplify(F);
        Trmn=solve(F,Trmn);
        TRM=double(Trmn);

        for j=1:length(TRM)
        if (imag(TRM(j))==0) & (real(TRM(j))>0)
            break
        end
        end

        Trm(i+1) = TRM(j);
        tlbulk(i+1)=Trm(i+1)*Tb;
        tiK(i) = ((ti(i)-32)*5/9)+273.15; %(deg. K)

        % Calculating the enthalpy of coolant
        Qc(i+1)=mlbulk(i)*hLm(i)+mvbulk(i)*hga(i) -mlbulk(i+1)*hLm(i+1)-mvbulk(i+1)*hga↙
```

```
(i+1);
        hLc(i+1)=Qc(i+1)/mc(i);

        syms Trc M;
        M=hLc(i+1)-(-R*Tb*1000*(-h_rol_w + Bw(1)*(T_ro_w - Trc) + Bw(2)/2*(T_ro_w^2 -
Trc^2) + Bw(3)/3*(T_ro_w^3 - Trc^3) - (Aw(1) + Aw(4)*Trc^2)*(Pr-P_ro_w) - Aw(2)/2*(Pr^2 -
P_ro_w^2)));
        simplify(M)
        Trc=solve(M,Trc);
        TRC=double(Trc);
        for j=1:length(TRC)
        if (imag(TRC(j))==0) & (real(TRC(j))>0)
            break
        end
        end

        tcout(i+1) = TRC(j);
        tc(i+1)=tcout(i+1)*Tb;
        Trc(i+1)=tcout(i+1);

        i=i+1;

end
```

LIST OF REFERENCES

1. Beutler, A., Greiter, I., Wagner, A., Hoffman, L., Schreier, S., Alefeld, G., 1996, "Surfactants and Fluid Properties," International Journal of Refrigeration, Vol.19(5), 342-346.

2. Bhavaraju, S.M., Russell, T.W.F., Blanch, H.W., 1978, "The Design of Gas Sparged Devices for Viscous Liquid Systems," AIChE Journal, ,Vol.24(3), 454-466.

3. Bogart, Marcel, 1981, Ammonia Absorption Refrigeration in Industrial Processes, Gulf Publishing Company, Texas.

4. Choudhury, S K., Hisajima, D., Ohuchi, T., Nishiguchi, A., Fukushima, T ., Sakaguchi, S., 1993, "Absorption of Vapors into Liquid Films Flowing over Cooled Horizontal Tubes," ASHRAE Transactions, Vol. 99(2), 81-89

5. Clift, R., Grace, J.R., Weber, M.E., 1978, Bubbles, Drops and Particles, Academic Press Inc., New York.

6. Conde Engineering, M., 2004, "Thermophysical Properties of {NH_3 H_2O} Solutions for the Industrial Design of Absorption Refrigeration Equipment, Formulation for Industrial Use," 1-34.

7. Conlisk, A T., 1992, "Falling Film Absorption on a Cylindrical Tube," AIChE Journal, Vol. 38(11), 1716-1728.

8. Conlisk, A T., 1994, "Structure of Falling Film Heat and Mass Transfer on a Fluted Tube," AIChE Journal, Vol. 40(5), 756-766.

9. Conlisk, A T., 1994, "Semi-analytical Design of a Falling film Absorber," Journal of Heat Transfer, Vol. 116, 1055-1058.

10. Conlisk, A T., 1995, "Analytical Solutions for the Heat and Mass Transfer in a Falling Film Absorber," Chemical Engineering Science, Vol.50(4), 651-660.

11. Conlisk, A Terrence, 1996, "Prediction of the Performance of a Spined-Tube Absorber- Part 1: Governing Equations and Dimensional Analysis," ASHRAE Transactions, Vol. 102(1), 110-121.

12. Conlisk, A Terrence,1996, "A Model for the Prediction of the Performance of a Spined-Tube Absorber – Part2: Model and Results," ASHRAE Transactions, Vol. 102(1), 122-131

13. Dahdal, Nadim, Grzetich, Deron, Jackson, Steven, Chadha, Satinderpal, "Absorption and Stripping," Senior Design CHE 396, NDSS Consulting. Web source: http://vienna.che.uic.edu/teaching/che396/sepProj/Absorption-NDSS.pdf. Last accessed: 04/22/2005.

14. Deckwer, W.-D., 1980, "On the Mechanism of Heat Transfer in Bubble Column Reactors," Chemical Engineering Science, Vol.35, 1341-1346.

15. Deckwar, W.-D., Schumpe, A., 1993, "Improved Tools for Bubble Column Reactor Design and Scale-up," Chemical Engineering Science, Vol.48(5), 889-911.

16. El-sayed, Y M., Tribus, M., 1985, "Therodynamic Properties of Water-Ammonia Mixtures: Theoretical Implementation for use in Power Cycle Analysis," ASME special publication: Analysis of Energy Systems, ASME AES Vol.1, 88-95.

17. Ferreira. C A. Infante, Keizer, C., Machielsen, C H M., 1984, "Heat and Mass Transfer in Vertical Tubular Bubble Absorbers for Ammonia-Water Absorption Refrigeration Systems," International journal of Refrigeration, Vol. 7 (6), 348-357.

18. Garimella, Srinivas, Coleman, John W., 1998, "Design of Cross-Flow Condensers for Ammonia-Water Absorption Heat Pumps," ASHRAE Transactions, Vol.104(1) 1553-1564.

19. Goel, Nitin, 2004, "A Theoretical and Experimental Analysis of Absorption-Condensation in a Combined Power-Cooling Cycle," Ph.D. Proposal, University of Florida.

20. Gosney, W B., 1982, Principles of Refrigeration, Cambridge University Press, Cambridge.

21. Goswami, Yogi, Xu, Feng, 1999, "Analysis of a New Thermodynamic Cycle for Combined Power and Cooling Using Low and Mid Temperature Solar Collectors," Journal of Solar Energy Engineering, Vol.121, 91-97.

22. Hasan, Afif Akel, Goswami, D Y., 2003, "Exergy Analysis of a Combined Power and Refrigeration Thermodynamic Cycle Driven by a Solar Heat Source," Journal of Solar Energy Engineering, Vol 125, 55-60.

23. Herbine, Gregory S., and Perez-Blanco, Horacio, 1995, "Model of an Ammonia-Water Bubble Absorber," ASHRAE Transactions, Vol. 101 (1), 1324-1332.

24. Hikita, H., Asai, S., Tanigawa, K., Segawa, K., Kitao, M., 1980, "Gas Hold-up in Bubble Columns," The Chemical Engineering Journal, Vol.20, 59-67.

25. Hikita, H., Asai, S., Tanigawa, K., Segawa, K., Kitao, M., 1981, "The Volumetric Liquid-Phase Mass Transfer Coefficient in Bubble Columns," The Chemical Engineering Journal, Vol.22, 61-69.

26. Ibrahim, O M., Klein, S A., 1993, "Thermodynamic Properties of Ammonia-Water Mixtures," ASHRAE Transactions, Vol.99 (1), 1495-1502.

27. Islam, Md. Raisul, Wijeysundera, N E., Ho, J C., 2003, "Performance Study of a Falling-Film Absorber with a Film-Inverting Configuration," International Journal of Refrigeration, Vol. 26, 909-917.

28. Jaeger Products Inc., "Fraction Tray and Hardware, Product Bulletin 400," Web source: http://www.jaeger.com/Brochure/400.pdf. Last accessed: 04/22/2005.

29. Jeong, Siyoung, Lee, Sang Kyoon, 1998, "Heat Transfer Performance of a Coiled Tube Absorber with Working Fluid of Ammonia/Water," ASHRAE Transactions, Vol.104 (1), 1577-1583.

30. Kang, Yong T., Christensen, Richard N., 1995, "Transient Analysis and Design Model of a LiBr-H_2O Absorber with Rotating Drums," ASHRAE Transactions, Vol. 101(1), 1163-1174.

31. Kang, Yong Tae, Chen, Weibo, Christensen, Richard N., 1996, "Design of Ammonia-Water Condenser with a Fluted Tube," ASHRAE Transactions, Vol.102(2), 587-595.

32. Kang ,Yong Tae, Christensen, Richard N., Kashiwagi, Takao, 1998, "Ammonia-Water Bubble Absorber with a Plate Heat Exchanger," ASHRAE Transactions, Vol. 104(1), 1565-1575.

33. Kang, Yong Tae, Akisawa, Atsushi, Kashiwagi, Takao, 2000, "Analytical Investigation of Two Different Absorption Modes: Falling Film and Bubble Types," International Journal of Refrigeration, Vol. 23, 430-443.

34. Kang, Y,T., Fujita, Y., Kashiwagi, T., 2001, "Combined Heat and Mass Transfer Under Different Inlet Subcooling Modes During NH_3-H_2O Falling Film Absorption Process," Transactions of the ASME, Vol.123, 242-249.

35. Kang,Yong Tae, Nagano,T., Kashiwagi, Takao, 2002, "Visualization of Bubble Behavior and Bubble Diameter Correlation for NH_3-H_2O Bubble Absorption," International Journal of Refrigeration, Vol. 25, 127-135.

36. Kiyomi, Akita, Yoshida, Fumitake, 1974, "Bubble Size, Interfacial Area, and Liquid Mass Transfer Coefficient in Bubble Columns," Industrial and Engineering Chemistry Process Design and Development, Vol.13 (1), 84-91.

37. Kumar, Akhilesh, Degaleesan, T.E., Laddha, G.S., Hoelscher, H.E., 1976, "Bubble Swarm Characteristics in Bubble Columns," The Canadian Journal of Chemical Engineering, Vol.54, 503-508.

38. Lerner, B J., Grove, C S., 1951, "Critical Conditions of Two-Phase Flow in Packed Columns," Industrial and Engineering Chemistry, Vol.43 (1), 216-225.

39. Lu, Shaoguang, Goswami, D Yogi, 2003, "Optimization of a Novel Combined Power/Refrigeration Thermodynamic Cycle," Journal of Solar Energy Engineering – Transactions of ASME, Vol. 125(2), 212-217.

40. Merrill, T L., and Perez-Blanco, H., 1997, "Combined Heat and Mass Transfer During Bubble Absorption in Binary Solutions," International Journal of Heat and Mass Transfer, Vol. 40 (3), 589-603.

41. Moller, R., Knoehe, K.F., 1996, "Surfactants with NH_3-H_2O," International Journal of Refrigeration, Vol.19(5), 317-321.

42. Norton, Ellis, 2001, "Ammonia Liquid Recirculation," ASHRAE Journal, Vol. 43(10), 50-51.

43. Park, Chan Woo, Kim, Sung Soo, Cho, Hyun Churl, Kang, Yong Tae, 2003, "Experimental Correlation of Falling Film Absorption Heat Transfer on Micro-Scale Hatched Tubes," International Journal of Refrigeration, Vol.26 (7), 758-763.

44. Patnaik, V., Perez-Blanco, H., Ryan, W A., 1993, "A Simple Analytical Model for the Design of Vertical Tube Absorbers,"ASHRAE Transactions, Vol. 99(2), 69-80.

45. Perez-Blanco, H., 1988, "A Model of an Ammonia-Water Falling Film Absorber," ASHRAE Transactions, Vol. 95(1), 467-483.

46. Perry, Robert H., and Chilton, Cecil H., 1973, Chemical Engineers' Handbook, Fifth Edition, Mc Graw-Hill, New York.

47. Rauschert Process Technologies, Web source: http://www.rauschertus.com/process_technologies/sievetrays.html . Last accessed: 04/22/2005.

48. Selim, A M., Elsayed, M M., 1999, "Interfacial Mass Transfer and Mass Transfer Coefficient in Aqua Ammonia Packed Bed Absorber," International Journal of Refrigeration, Vol. 22, 263-274.

49. Selim, A M., Elsayed, M M., 1999, "Performance of a Packed Bed Absorber for Aqua Ammonia Absorption Refrigeration System," International Journal of Refrigeration, Vol. 22, 283-292.

50. Shah, Y.T., Kelkar, B.G., Godbole, S.P., Deckwer, W.-D. 1982, "Design Parameters Estimations for Bubble Column Reactors," AIChE Journal, Vol.28(3), 353-379.

51. Sherwood, T K., Shipley, G H ., Holloway F.A., 1938, "Flooding Velocities in Packed Columns," Industrial and Engineering Chemistry, Vol.30(7), 765-769.

52. Smith, 1963, Design of Equilibrium Stages Processes, Mc Graw Hill, New York.

53. Staicovici, M D., 2000, "A Non-equilibrium Phenomenological Theory of the Mass and Heat Transfer in Physical and Chemical Interactions Part II- Modeling of the NH_3/H_2O Bubble Absorption, Analytical Study of Absorption and Experiments," International Journal of Heat and Mass Transfer, Vol.43, 4175-4188.

54. Stichlmair, J G., Fair, J R., 1998, Distillation, Principles and Practices, Wiley-Liss publication, New York.

55. Sujatha, K S., Mani, A., Murthy, S Srinivasa, 1999, "Experiments on a Bubble Absorber," International Communications in Heat and Mass Transfer, Vol. 26 (7), 975-984.

56. Summerer, Franz, Ziegler, Felix, Riesch, Peter, Alefeld, Georg, 1996, "Hydroxide Absorption Heat Pumps with Spray Absorber," ASHRAE Transactions, Vol.102 (1), 1010-1016.

57. Tamm, Gunnar, Goswami, D Y., Lu, Shaoguang, Hasan, Afif Akel, 2002, " A Novel Combined Power and Cooling Thermodynamic Cycle for Low Temperature Heat Sources – Part I: Theoretical Investigation," Journal of Solar Energy Engineering – Transactions of ASME, Vol. 125(2), 218-222.

58. Tamm, Gunnar, Goswami, D Y., 2002, "A Novel Combined Power and Cooling Thermodynamic Cycle for Low Temperature Heat Sources – Part II: Experimental Investigation," Journal of Solar Energy Engineering – Transactions of ASME, Vol. 125(2), 223-229.

59. Tamm, Gunnar Olavi, 2003, "Experimental Investigation of an Ammonia-Based Combined Power and Cooling Cycle," Ph.D. Dissertation, University of Florida.

60. Tham, Ming T., 1997, Distillation, Web Source : http://lorien.ncl.ac.uk/ming/distil/distilint.htm. Last accessed: 04/22/2005.

61. Treybal, R E, 1955, Mass Transfer Operations, Mc Graw Hill publications, New York.

62. Wijn, E. Frank, 2001, "Trays in More Detail," Web Source: http://www.euronet.nl/users/wijnef/public_html/TrDetail.html. Last accessed: 04/22/2005.

63. Xu, Feng, Goswami, D Y., 1999, "Thermodynamic Properties of Ammonia-Water Mixtures for Power-Cycle Applications," Energy, Vol.24, 525-536.

64. Xu, Feng, Goswami, D Y., Bhagwat, Sunil S., 2000, " A Combined Power/Cooling Cycle," Energy, Vol. 25, 233-246.

65. Ziegler, B., and Trepp, Ch., 1984, "Equation of State for Ammonia-Water Mixtures", International Journal of Refrigeration, Vol. 7 (2), 101-106.

BIOGRAPHICAL SKETCH

Sirisha Devi Govindaraju was born on October 7th, 1981, in Hyderabad, the Pearl City of India. She received all her education in Hyderabad before embarking on the journey to the United States. She graduated from Osmania University, Hyderabad, in June 2003 where she obtained her bachelor's in mechanical engineering. She will graduate with a Master of Science in mechanical and aerospace engineering from the University of Florida in August 2005.